Agricultural Water Management 325 (2026) 110157

Contents lists available at ScienceDirect

Agricultural Water Management

journal homepage: www.elsevier.com/locate/agwat

Spatio-temporal HYDRUS-1D soil water balance simulations as support for precision irrigation in North-Eastern Germany

Jan Lukas Wenzel [a,*], Christopher Conrad [a], Talha Mahmood [a], Matthias Kunz [b], Martin Volk [c], Julia Pöhlitz [a]

[a] Department of Geoecology, Institute of Geosciences and Geography, Martin Luther University Halle-Wittenberg, Halle (Saale) 06120, Germany
[b] Department of Geodesy & Remote Sensing, GFZ German Research Centre for Geosciences Potsdam, Telegrafenberg, Potsdam 14473, Germany
[c] Department of Computational Landscape Ecology, UFZ Helmholtz Centre for Environmental Research, Leipzig 04318, Germany

ARTICLE INFO

Handling Editor - Xiying Zhang

Keywords:
HYDRUS-1D
Plant available water content
Irrigation efficiency
Soil moisture active and passive
Sentinel-1 soil water content

ABSTRACT

Accurate spatio-temporal information on the soil water balance is critical for an efficient and sustainable irrigation. Large effort requirements limit the applicability of complex simulations for precision irrigation. The spatially distributed application of one-dimensional models can reconcile the need for precise soil water balance simulations with the complexity of root-zone water flow processes. This study uses HYDRUS-1D to simulate the daily depth-specific (0 cm to 60 cm, in 10 cm increments) soil water balance from 1st April to 30th September 2021 (2022). Simulations at 70 m spatial resolution covered a 1600 ha farm in Mecklenburg-Western Pomerania, Germany. Results were validated against in-situ soil water content (SWC) and two remotely-sensed SWC data sets ("Soil Moisture Active Passive", SMAP; Sentinel-1, S1-SWC). Further analysis explored crop-specific irrigation efficiencies and potential farm-scale water savings. Spatially distributed HYDRUS-1D simulations showed good accuracy compared to in-situ SWC ($RMSE_{mean} = 0.020\ m^3\ m^{-3}$; $MAE_{mean} = 0.017\ m^3\ m^{-3}$; $R^2_{mean} = 0.676$; bias = $-0.008\ m^3\ m^{-3}$). The agreement with remotely-sensed SWC was moderate to weak ($RMSE_{mean} = 0.059$ (0.150) $m^3\ m^{-3}$, $MAE_{mean} = 0.049$ (0.123) $m^3\ m^{-3}$, $R^2_{mean} = 0.208$ (0.141), mean bias = 0.021 (0.108) $m^3\ m^{-3}$ for SMAP (S1-SWC)). Irrigation efficiencies were 65.0 % (potato), 47.3 % (wheat), 40.5 % (rye), and 58.2 % (sugar beet). Potential water savings amounted to 87,006.9 m^3 (11.2 % of total irrigation water; 2021) and 71,396.6 m^3 (10.4 %; 2022). The proposed approach reduces the trade-offs between accurately representing the soil water balance in the root-zone and keeping the practical effort reasonable.

1. Introduction

Irrigation is required in many parts of the world to maintain crop productivity and to optimize yield and the quality of the crop. Also in the humid and temperate regions of Central Europe, irrigation is an important strategy to replenish and maintain the soil water content

Abbreviations: ANOVA, analysis of variance; BD, dry bulk density; CWR, crop water requirements; DEMMIN, Durable Environmental Multidisciplinary Monitoring Information Network; E_a, actual evaporation; E_p, potential evaporation; ET_0, FAO-56 Penman-Monteith reference evapotranspiration; ET_C, crop evapotranspiration; IE_{ETC}, irrigation efficiency with the use of crop evapotranspiration; IE_{Ta}, irrigation efficiency with the use of crop transpiration; HSD, Tukey honestly significant difference test; HYDRUS-1D-SWC, SWC derived from spatially distributed HYDRUS-1D simulations; I_{gross}, gross irrigation depth; I_{used}, sum of irrigation water beneficially used by the crop; Kh, pressure head dependent unsaturated hydraulic conductivity; K_{Sat}, saturated hydraulic conductivity; LAI, leaf area index; MAE, Mean Absolute Error; MODIS, Moderate Resolution Imaging Spectroradiometer; PAW, plant available water content; PI, precision irrigation; R^2, coefficient of determination; RMSE, Root Mean Square Error; RS, remote sensing; RSE, residual standard error; S1-SWC, Surface soil water content observed with Sentinel-1 C-Band radar; SAR, Synthetic Aperture Radar; S_e, effective saturation; SMAP, Soil Moisture Active and Passive; SMAP-1km, downscaled 1 km SMAP soil water content; SWC, soil water content; T_a, actual transpiration; T_p, potential transpiration; VGM, van Genuchten-Mualem functional relationship; θh, pressure head dependent soil water retention; θ_{33}, soil water content at a pressure head of h = -33 kPa; θ_{FC}, soil water content at field capacity; θ_{PWP}, soil water content at permanent wilting point; θ_r, residual soil water content; θ_{Sat}, volumetric soil water content at saturation.

* Correspondence to: Department of Geoecology, Institute of Geosciences and Geography, Martin Luther University Halle-Wittenberg, von-Seckendorff-Platz 4, Halle (Saale) 06120, Germany.

E-mail addresses: jan.wenzel@geo.uni-halle.de (J.L. Wenzel), christopher.conrad@geo.uni-halle.de (C. Conrad), talha.mahmood@student.uni-halle.de (T. Mahmood), matthias.kunz@gfz.de (M. Kunz), martin.volk@ufz.de (M. Volk), julia.poehlitz@geo.uni-halle.de (J. Pöhlitz).

https://doi.org/10.1016/j.agwat.2026.110157
Received 17 August 2025; Received in revised form 26 November 2025; Accepted 14 January 2026
Available online 5 February 2026
0378-3774/© 2026 The Author(s). Published by Elsevier B.V. This is an open access article under the CC BY license (http://creativecommons.org/licenses/by/4.0/).

(SWC) in the root-zone during temporal water scarcity (Rey et al., 2016). In recent years, agriculture in these typically rainfed biomes faces a negative climatic water balance during the growing season. For instance, North-Eastern Germany shows an average deficit of 140 mm during the growing season (April to September) for the period 1991–2020 (German Meteorological Service, 2024), which is accompanied by an increasing frequency of moderate to severe SWC deficits in the root-zone of the crop (Ionita and Nagavciuc, 2021). Here, originally sufficient natural freshwater resources allowed farmers to raise the gross irrigation depth (I_{gross}) to compensate for unproductive water losses during irrigation (Petrović et al., 2024). During low rainfall years, farmers already extracted up to ~125 % of the authorized groundwater volume for irrigation, signalling a clear vulnerability to temporal water deficits (Riediger et al., 2014). Although landscape patches due to the glacial development in North-Eastern Germany resulted in spatially varying soil properties and phenological characteristics, often within individual fields (Ehrhardt et al., 2025), the irrigated area is often considered as a homogeneous unit. In the light of the already apparent constraints of climate change, there is a strong need to adjust the values of I_{gross} to the actual crop water requirements (CWR).

In this context, precision irrigation (PI) aims at an accurate and location-specific characterization of CWR (Haghverdi et al., 2016; Pierce, 2010) and has hence emerged as a strategy with great potential for making an ecologically and economically feasible contribution to an efficient and sustainable water supply. Recent advantages in PI particularly include the optimization of existing irrigation techniques to enhance the technical-related application efficiency and to minimize unproductive water losses (Chauhdary et al., 2024). To accurately estimate CWR across spatio-temporal scales, PI basically requires precise information on different components of the depth-specific soil water balance in addition to SWC (e.g., plant available water content (PAW), crop evapotranspiration (ETc), subsurface fluxes, root water uptake) to enhance an assessment of the irrigation performance (e.g., by estimates of the irrigation efficiency or potential water savings). Here, previous approaches mainly aim to minimize the complexity of CWR and SWC estimations for implementation into agricultural practice (e.g., by smart sensors, Internet-of-Things networks, artificial intelligence and machine learning approaches, or GPS-controlled irrigation techniques). While simple-to-use in-situ sensors, such as Time Domain Reflectometry probes or Cosmic-Ray Neutron sensors, provide a high accuracy at the point or local scale, they often fail to capture the in-field specific variability of CWR due to costs and maintenance requirements (Phillips et al., 2014). These shortcomings of in-situ measurements in capturing the high spatio-temporal variability of SWC require advanced observation and modeling approaches, ranging from the non-contact and regular mapping of SWC through microwave remote sensing (RS-SWC), to relatively simple ET_C-based models (e.g., the FAO-56 dual crop coefficient method (Allen et al., 1998) or the "soil-water-balance code" (Westenbroek et al., 2018)), process-based crop models (e.g., DSSAT; Jones et al., 2003), and complex, physics-based numerical soil water balance simulations.

Numerous satellite-based platforms and sensors for microwave remote sensing are an important source of information as they allow for the non-contact and regular mapping of SWC a spatial resolution between 1 km and > 10 km (Fig. 1; Huang et al., 2025), based on the sensitivity of microwave backscatter to soil dielectric properties (Wang and Qu, 2009). Although advantageous in their usually free availabilty, the use of microwave RS-SWC for PI purposes is often limited to (i) a representation of solely surface (~0 cm - 5 cm) SWC, and (ii) a coarse spatial resolution, which does not support irrigation decisions at the local or in-field specific scale (Senanayake et al., 2024). Solely mapping surface SWC does not provide sufficient information for PI, since depth-specific SWC is more important for crop growth (Li et al., 2023). In this context, approaches to link surface RS-SWC with the infiltration process, such as the exponential filter method (Wagner, 1998) and the resulting "Soil Water Index", provide accurate estimates of depth-specific SWC on the global scale (Bauer-Marschallinger et al., 2018). However, the suitability of both the "Soil Water Index" and freely available RS-SWC data sets for PI purposes is limited to a coarse spatial resolution. For instance, the "Soil Moisture Active and Passive" (SMAP)

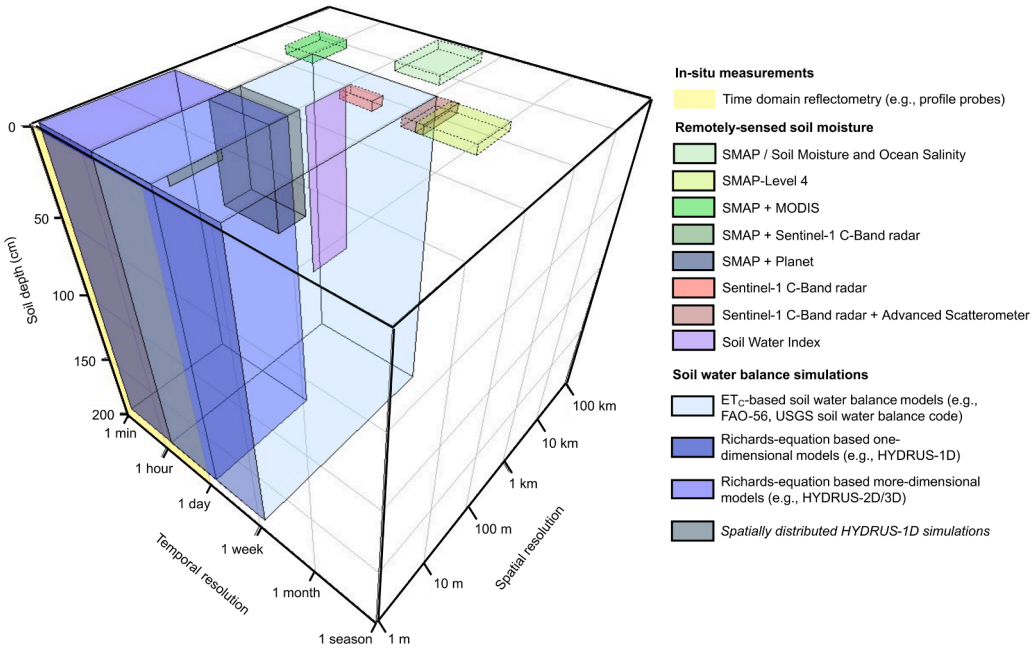

Fig. 1. Overview of the temporal and spatial resolution and reflected soil depth (cm) of selected methods for determining or simulating the soil water content (SWC). Different green colors indicate SWC data derived from the "Soil Moisture Active and Passive" (SMAP) product. Different red colors indicate SWC data derived from the Sentinel-1 C-Band radar. The purple box indicates the "Soil Water Index". Each remotely-sensed SWC data set is described in detail in Huang et al. (2025). Different blue colors indicate soil water balance simulations based on estimating the crop evapotranspiration (ET_C; e.g., the FAO-56 method or the USGS's soil water balance code) or on solving the Richards equation (e.g., HYDRUS-1D and HYDRUS-2D/3D) and the proposed approach for the spatially distributed application of HYDRUS-1D (written in italic). Note that remotely-sensed SWC data sets include both freely available and commercially available data.

product according to Fang et al. (2022), or the first global Sentinel-1 based SWC product (S1-SWC) according to Fan et al. (2025a), b) are provided at a spatial resolution of 1 km, resulting in a mismatch between the pixel size and field borders and spatial heterogeneities in environmental conditions such as soil properties, for instance. Novel algorithms for downscaling the raw satellite imagery to higher spatial resolution may offer far-reaching benefits for drought monitoring and irrigation scheduling (e.g., Conrad et al., 2020; El Hajj et al., 2017; Mahmood et al., 2024; Tola et al., 2025).

From a modeling perspective, simple ET_C-based models primarily emphasize the derivation of CWR as the water consumption from the soil through soil evaporation and crop transpiration (Pereira et al., 2020) but simplify the complex water flow processes in the root-zone (e.g., root water uptake, capillary rise, deep percolation). Here, also multispectral or thermal RS data at high spatial resolution are an important source of information for a spatially distributed application of these models (Gu et al., 2020). Due to simplicity in application, these approaches are widely used in agricultural practice for irrigation scheduling (Tenreiro et al., 2020). Process-based crop models primarily focus on simulating the crop growth and yield response but usually also simplify the complex processes of water flow dynamics in the root-zone of the crop. In contrast, complex soil water balance simulations (e.g., based on a numerical solution of the Richards equation, such as the HYDRUS model framework (Šimůnek et al., 2012a, b)) offer high accuracy in describing the water flow dynamics within the root-zone, solute transport and root water uptake under complex boundary conditions (Ghazouani et al., 2019; Kandelous and Šimůnek, 2010), and are hence increasingly included in irrigation decisions. However, their practical use across large and spatially heterogeneous sites as support for PI is typically limited due to high computational effort requirements and extensive input data demands. Consequently, previous studies have been restricted to individual fields or homogeneous test sites and have seldom integrated spatially heterogeneous soil properties, meteorological conditions, spatially varying values of I_{gross} and phenological characteristics at an operational management scale.

Despite progress in PI technologies, no operational approach exists that simultaneously (i) represents the spatial variability in soil properties, meteorological conditions, gross irrigation depths, and phenological characteristics, (ii) captures depth-specific processes of water flow dynamics, and (ii) operates at a spatial resolution relevant for the purpose of PI. Here, one-dimensional numerical soil water balance simulations (namely HYDRUS-1D, Šimůnek et al., 2005) also precisely simulate different components of the soil water balance (SWC, PAW, ET_C, subsurface fluxes, root water uptake) with feasible computational efforts (see Er-Raki et al., 2021; Kumar et al., 2022; Wenzel et al., 2025, for instance), but with respect to vertical water flow dynamics. An application of HYDRUS-1D in a spatially distributed manner, however, may critically balance the trade-offs of other approaches between a precise simulation of different components of the soil water balance with the scale of application and computational feasibility. Although already tested on the field or regional scale in comparison to two-dimensional or three-dimensional simulations (Mao et al., 2021; Rezaei et al., 2017), so far, the potential of this approach with regard to any spatially heterogeneous values of I_{gross} and environmental conditions has not been systematically evaluated in comparison to in-situ measurements and RS-SWC under real farm-scale conditions and for practical PI decision-making.

This study is designed to bridge this gap of comprehensive analyses of in-situ measured, remotely-sensed and simulated SWC across spatio-temporal scales by implementing a framework for spatially distributed HYDRUS-1D soil water balance simulations at a spatial resolution of 70 m. This spatial resolution is in line with the average working width of the gun sprinkler irrigation systems often utilized for supplemental irrigation of high-value crops under humid climate conditions. With a particular emphasis given on a farm in the Durable Environmental Multidisciplinary Monitoring Information Network" (DEMMIN) site (Spengler et al., 2021) within the heterogeneous landscape of North-Eastern Germany, the objective of this study is three-fold:

1. HYDRUS-1D is applied in a spatially distributed manner across all fields of an existing farm, explicitly via a-priori information on depth-specific soil physical properties, weather conditions, location-specific values of I_{gross}, and phenological characteristics, to derive accurate depth-specific simulations of different components of the soil water balance (SWC, PAW, ET_C, subsurface fluxes, root water uptake).
2. The accuracy of the simulated components of the soil water balance is evaluated using in-situ measurements and two freely available RS-SWC data sets (SMAP-1km, Fang et al. 2022; S1-SWC, Fan et al. 2025a, b)) to enable a comprehensive accuracy assessment of different approaches considered for the purpose of PI.
3. To explore the suitability and contribution of spatially distributed HYDRUS-1D simulations for the purpose of PI, the validated components of the soil water balance are used to derive reliable irrigation performance indicators (irrigation efficiency, potential water savings).

2. Material and methods

2.1. Study area characterization

This study was conducted from 1st April to 30th September in two years, 2021 and 2022, on all fields of a farm (cultivated area: 1600 ha) near the village of Bentzin, Mecklenburg-Western Pomerania, Germany within the DEMMIN site (Fig. 2). Cultivated crops include potatoes, winter cereals (wheat, barley, rye), winter rapeseed, sugar beet and lupins (Table 1). All crop management procedures were conducted by the local farmer in accordance with standard agronomic practices (Burth and Freier, 1999). The agricultural focus is on potato production, with an area used for growing potatoes of 895.9 ha (564.2 ha) in 2021 (2022).

The soils in the farmyard are typical of the glacially formed landscape in Central Europe, with varying soil properties within individual fields (Fig. 2). According to the "Reichsbodenschätzung"[1]; (Görz and Hock, 1939), the predominant soil textures are loamy sand (28.0 % of the total area, 44.5 %, and 16.8 % for the different soil textural classes) and the pure sand (9.1 %), locally alternating with sandy loams (0.7 %), clayey soils (0.1 %), peatlands (0.6 %) and kettle holes (0.2 %; Fig. 2). The predominant soil type is a stagnic Cambi-/Luvisol, locally alternating with Cambi-/Luvisols and Cambisols, corresponding to the "World Reference Base for Soil Resources" (IUSS Working Group WRB, 2015). The relief across the study farm is relatively even, with an average slope of 1.52°.

The long-term (period 1991–2020) average air temperature in the study region ranges between 0.9 °C in January and 18.6 °C in July (climate station "Greifswald"; German Meteorological Service, 2024). In the same period, the long-term annual precipitation amounted to 601.0 mm and ET_0 was 582.3 mm, respectively. The annual precipitation ranged between 438.4 mm in 1996 and 848.5 mm in 2010 and ET_0 ranged between 489.2 mm in 1996 and 724.7 mm in 2018. During the study period from 1st April to 30th September 2021 (2022), the average air temperature was 14.4 °C (15.3 °C). Precipitation amounted to 296.1 mm (232.5 mm) and the average wind speed was 7.5 m s^{-1} (6.8 m s^{-1}). ET_0 amounted to 522.1 mm (564.1 mm; Table 2) during the study period and was hence higher than the long-term (period

[1] The "Reichsbodenschätzung" is a German agricultural soil map used for tax purposes. The soil textures of the "Reichsbodenschätzung" were in good agreement (85.6 %) with soil textures determined in the laboratory (laser diffraction method; Helos/KR, Sympatec GmbH, Clausthal-Zellerfeld, Germany) of disturbed topsoil (0 cm to 30 cm) samples (N = 373) collected from all fields.

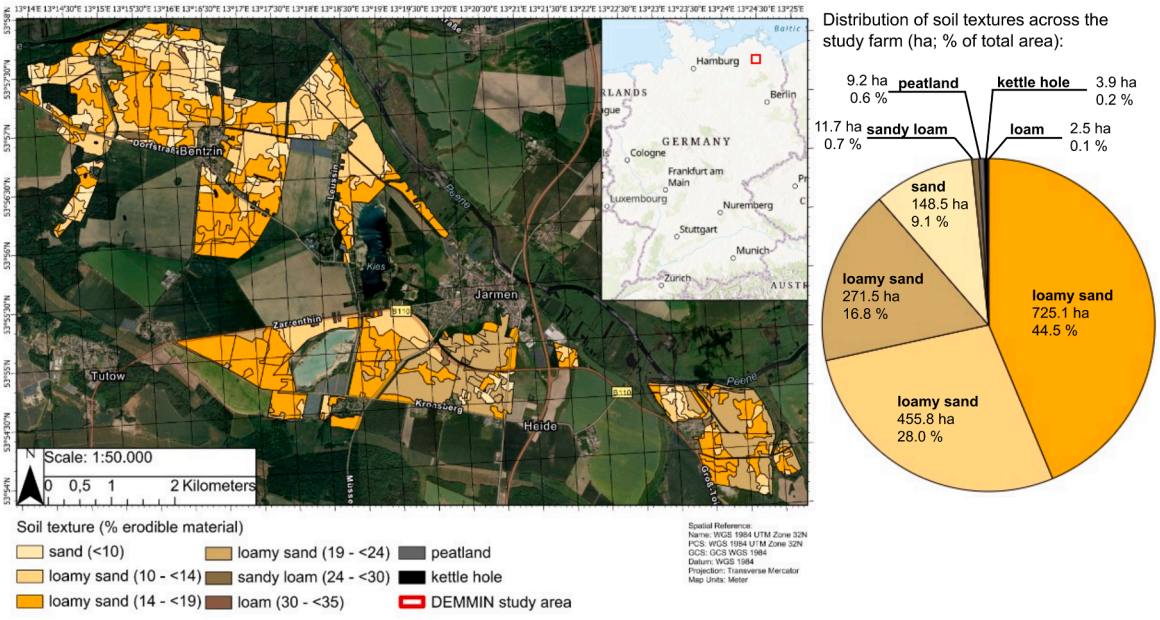

Fig. 2. Soil textures on the fields of the farm in Mecklenburg-Western Pomerania (cultivated area: ~1600 ha) within the DEMMIN study area (red border), according to the "Reichsbodenschätzung" (Görz and Hock, 1939). The soil textures in the "Reichsbodenschätzung" are classified according to the proportion of erodible material (i.e., particles with a mean diameter of <0.01 mm). The thresholds of the proportion of erodible material for each soil textural class are shown in brackets. The distribution (total area, ha; % of total area) of each soil texture across the study farm are shown on the right side. The dominating soil textures are the loamy sand and the pure sand, alternating with sandy loams, clayey soils, peatlands and kettle holes.

Table 1
Cultivated area (ha, % of total cultivated area)) per crop in 2021 and 2022, including maximum crop height (cm), maximum rooting depth (cm), seasonal sums of the gross irrigation depth (mm; I_{gross}), and optimum ranges of plant available water content (%) for each crop. The phenological characteristics (maximum crop height, maximum rooting depth, crop-specific optimum ranges of plant available water content) were derived from standard values implemented in commonly used irrigation decision support systems in German irrigated agriculture ("ZEPHYR", Michel and Dannowski, 2013; "agrowetter beregnung", German Meteorological Service, 2017), which are also used by the local farmer for irrigation scheduling.

Crop	Cultivated area				Maximum crop height (cm)	Maximum rooting depth (cm)	I_{gross} (mm)[3,4]		Optimum ranges of plant available water content (%)	
	2021		2022				2021	2022	Early growth stage	Later growth stage
	(ha)	(%)	(ha)	(%)						
Potato	895.9	55.1	564.2	34.7	90	80	79.0	92.8	40–80	50–90
Wheat	361.1	22.1	355.1	21.8	140	120	17.9	32.2	50–65	40–60
Barley	75.7	4.7	157.2	9.7	100	120	0.0	0.0	50–65	40–60
Rye	71.0	4.4	86.3	5.3	120	120	3.2	6.9	50–65	40–60
Rapeseed	139.9	8.6	314.1	19.3	140	150	0.0	0.0	50–60	40–60
Sugar beet	48.3	3.0	104.9	6.4	80	160	0.0	16.8	20–80	50–80
Lupin	36.6	2.3	46.6	2.9	90	160	0.0	0.0	55–90	50–90
Applied irrigation water (m^3)[5]							774,670	661,498		

[3]Location-specific values of I_{gross} were derived from 7-min GPS-based speed and operating pressure information of the utilized traveling gun sprinkler irrigation system.
[4]Crop-specific sums of I_{gross} were derived by summarizing the location-specific values over the entire growing season (April to September) and calculating the average value for each crop across the respective fields across the study farm.
[5]The farm-scale sum of irrigation water (m^3) applied was determined by accumulating the location and event-specific values of I_{gross} for all crops and the area used for growing each crop.

Table 2
Meteorological conditions from 1st April to 30th September 2021 and 2022, according to the spatially distributed daily meteorological datasets (German Meteorological Service, 2024), which were used for spatially distributed soil water balance simulations: T_{mean} = average air temperature (°C), T_{min} = minimum air temperature (°C), T_{max} = maximum air temperature (°C), Prec = precipitation (mm), $Prec_{eff}$ = effective precipitation (mm), $Prec_{eff\%}$ = percent effective precipitation of total precipitation (%), U = wind speed (m s^{-1}), ET_0 = FAO-56 Penman-Monteith reference evapotranspiration (mm). $Prec_{eff}$ was calculated according to the FAO-CROPWAT approach (Smith, 1992).

	T_{mean} (°C)	T_{min} (°C; Date)	T_{max} (°C; Date)	Prec (mm)	$Prec_{eff}$ (mm)	$Prec_{eff\%}$ (%)	U (m s^{-1})	ET_0 (mm)
2021	14.4	2.3 (7th April)	26.0 (19th June)	296.1	239.4	80.9	7.5	522.1
2022	15.3	0.6 (2nd April)	28.1 (24th August)	232.5	192.2	82.7	6.8	564.1

1991–2020) average ET_0 from 1st April to 30th September (504.4 mm, with ranges from 428.6 mm in 1996–628.6 mm in 2018; German Meteorological Service, 2024).

Gun sprinkler irrigation systems (Fasterholt FM 4900 H, Fasterholt Maskinfabrik A/S, Brande, Denmark) are used on all irrigated fields of the farm (total area equipped for irrigation: 1468.7 ha, 91.5 %). These systems are among the most frequently used irrigation techniques in Central Europe due to their advantage of replenishing and maintaining SWC in the root-zone during short-term water shortages by applying large values of I_{gross} between 35 mm and 40 mm at relatively low installation and maintenance costs. These advantages are of particular importance for an economically feasible irrigation of water-consumptive crops (e.g., grain maize, rice, potatoes) on heterogeneous sites. The average diameter of throw in a half circle was approximately 72 m, which corresponds to an irrigation set (i.e., the area that is irrigated at one time) of approximately 2035 m^2. Nonetheless, the application efficiency (i.e., the ratio of irrigation water stored within the root-zone), is expected to range from 50 % to 70 %, based on look-up tables or manuals (see Wenzel et al., 2025, for a detailed description), and is hence lower than with other irrigation techniques (e.g., center pivot or drip irrigation systems). Unproductive water losses of gun sprinkler irrigation systems are mainly related to surface runoff, deep percolation, wind drift and spray evaporation, and interception, among others.

Crop-specific net irrigation depths were iteratively scheduled by the local farmer using ZEPHYR (Michel and Dannowski, 2013), a commonly tool for irrigation scheduling in Germany. The exact values of I_{gross} were derived from raw 7-min GPS-based speed and operating pressure data of the utilized gun sprinkler irrigation system, which were provided by the irrigation performance monitoring software "Raindancer Smart Irrigation Management" (IT-Direkt Business Technologies GmbH, Berlin, Germany), which is used by the farmer. Based on these raw irrigation performance data, the application rate (in $m^3\ h^{-1}$) is automatically calculated and provided by the "Raindancer Smart Irrigation Management" software. Based on a conversion table provided by the technical manual of the utilized gun sprinkler irrigation system, the location-specific values of the application rate were transformed to location-specific (i.e., 7-min) values of I_{gross}, as dependent on the nozzle diameter (in this study a nozzle with an inside diameter of 1.1" was used). These derived values of I_{gross} were spatially aggregated and rasterized to a spatial resolution of 70 m, according to the average diameter of throw of the traveling gun sprinkler irrigation systems. The overall average sums of I_{gross} are shown in Table 1 for each crop and year.

2.2. Soil water balance simulations

2.2.1. Conceptualization

Soil water balance simulations were conducted at daily time steps from 1st April to 30th September 2021 and 2022 (183 time steps per year; Fig. 3) using the physically-based HYDRUS-1D software environment (Version 4.00; Šimůnek et al., 2005). Different components of the soil water balance (SWC, PAW, ET_C, infiltration, root water uptake) were simulated at "observation nodes" at 0 cm to 60 cm depths, in 10 cm increments, by solving the highly nonlinear Richards equation (Richards, 1931):

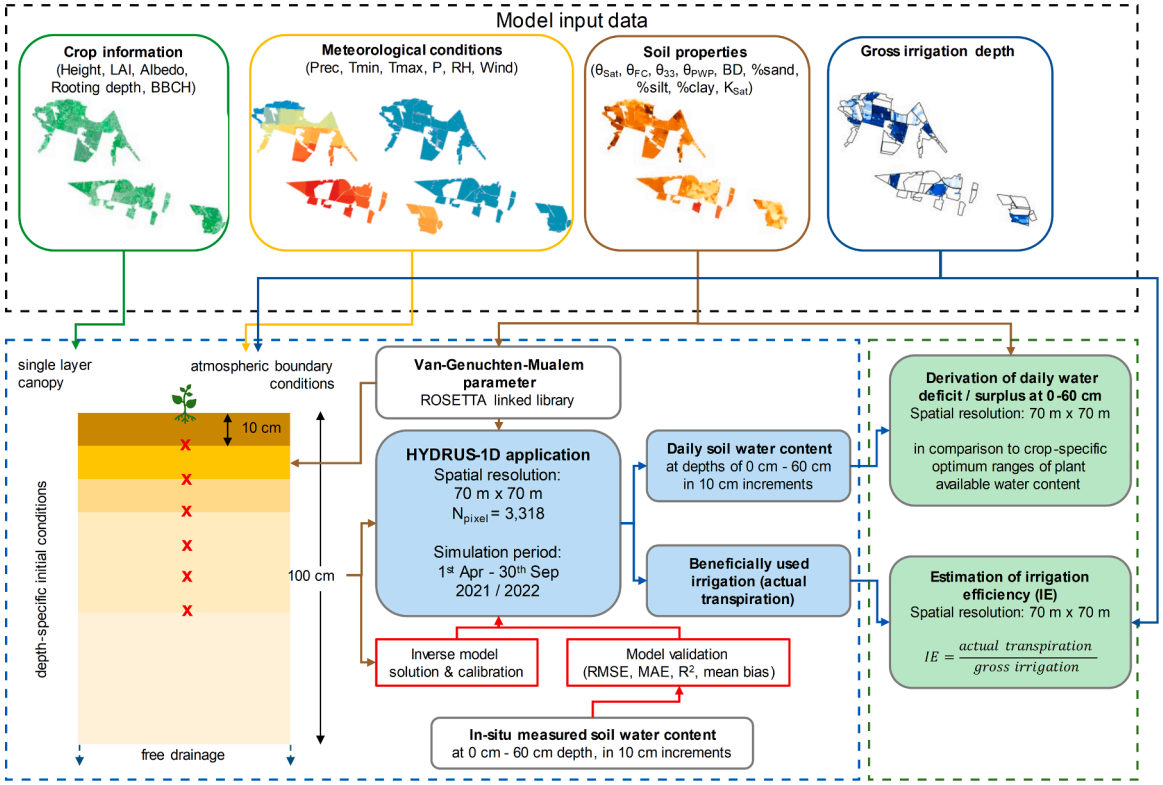

Fig. 3. Conceptualization and parameterization (black dashed box), processes (blue dashed box) and applications (green dashed box; farm-scale water savings, irrigation efficiency) of spatially distributed soil water balance simulations at six different depths (red crosses: 0 cm to 60 cm, in 10 cm increments) from 1st April to 30th September 2021 and 2022 with daily time steps (total time steps: 183). The HYDRUS-1D software environment was applied at a spatial resolution of 70 m (N = 3318) using the "hydrusR" (Acharya, 2020) package in "RStudio" (Version 1.4). Different arrow colors indicate different groups of input and output data: green - crop information (crop height, leaf area index (LAI), rooting depth, growth stage (BBCH)); yellow - meteorological conditions (precipitation (Prec), minimum and maximum air temperature (Tmin, Tmax), air pressure (P), relative humidity (RH), wind speed); brown - soil properties (soil water content at saturation (θ_{Sat}), field capacity (θ_{FC}), h = -33 kPa (θ_{33}), and permanent wilting point (θ_{PWP}), dry bulk density (BD), soil textural classes (%sand, %silt, %clay), and saturated hydraulic conductivity (K_{Sat})); red - calibration and validation; blue - simulated soil water content and post-processing.

$$\frac{\delta\Theta}{\delta t} = \frac{\delta}{\delta z}\left(K(h)\frac{\delta h}{\delta z}\right) + \frac{\delta K(h)}{\delta z} - S(h) \quad (1)$$

where θ is the volumetric SWC ($L^3\,L^{-3}$), h is the pressure head (L), t is time (T), z is the spatial coordinate (L; positive upward), K(h) is the unsaturated hydraulic conductivity ($L\,T^{-1}$), and S(h) is a sink term accounting for the pressure-head dependent root water uptake ($L^3\,L^{-3}\,T^{-1}$).

A spatially distributed application of one-dimensional soil water balance simulations with HYDRUS-1D requires that the area to be simulated is considered as a composite of one-dimensional soil columns. The soil profile in each 1D soil column was discretized into five layers (Fig. 3; 0 cm to 10 cm, 10 cm to 20 cm, 20 cm to 30 cm, 30 cm to 60 cm, 60 cm to 100 cm), according the combined a-priori information on the soil physical properties which were used as input data (Section 2.2.2). This soil layer discretization has been validated in the field and is independent of the pre-defined observation nodes at soil depths of 0 cm to 60 cm, in 10 cm increments (Šimůnek et al., 2005).

A spatial resolution of 70 m was chosen for the simulations, according to the average diameter of throw of the traveling gun sprinkler irrigation system used. The farm was therefore divided into a total of 3318 1D soil columns (Fig. 3). The following assumptions are necessary for simulating complex water flow processes within the root-zone using 1D soil columns (Kuznetsov et al., 2012; Rezaei et al., 2017):

(i) Lateral flow within each 1D soil column and between different 1D soil columns is considered negligible, which allows for parallel parameterization,
(ii) A freely draining lower boundary condition is assumed in each 1D soil column, which is justified for the study region owing to a groundwater table below a depth of 3 m, and
(iii) Effects of the topography (terrain surface or slope) on the soil water balance are considered negligible.

All soil water balance simulations were performed successively for each 1D soil column by running HYDRUS-1D in a batch process using the "hydrusR" package (Version 0.3.0.; Acharya, 2020) in the open-source software "RStudio" (Version 1.4., RStudio Team, Boston, MA, USA), as an integrated development environment for "R" (Version 4.1.1.).

2.2.2. Parameterization

Soil layer specific unsaturated soil hydraulic properties were estimated based on the functional dependency between the pressure head and the unsaturated SWC according to van Genuchten (1980); App. A: Eq. A1) and the predictive pore-size distribution equation according to Mualem (1976); Eq. A2), hereinafter referred to as the "van Genuchten-Mualem (vGM) model". The vGM model consists of seven different parameters, in total: the volumetric SWC at saturation (θ_{Sat}), the saturated hydraulic conductivity (K_{Sat}), the residual SWC (θ_r), and four empirical fitting parameters (α, n, m, l), although the parameter m is usually defined as

$$m = 1 - \frac{1}{n}, \quad (2)$$

for $n > 1$ (Kool et al., 1987), and l was defined as $l = 0.5$ (Mualem, 1976).

θ_r, α and n were estimated using the ROSETTA pedotransfer function (Schaap et al., 2001), which is implemented in the "SoilDB" package (Version 2.8.3; Beaudette et al., 2024) in "RStudio". This pedotransfer function is generally considered as providing accurate estimates of vGM parameters for various soil and meteorological conditions (Vereecken et al., 2010). ROSETTA requires depth-specific information on soil textural classes (% sand, % silt, % clay), dry bulk density (BD), volumetric SWC at a pressure head of h = -33 kPa (θ_{33}), and volumetric SWC at permanent wilting point (θ_{PWP}).

Hence, a numerical solution of the vGM model with the ROSETTA pedotransfer function requires a total of six soil physical properties (Fig. 3): θ_{Sat}, K_{Sat} as parameters of the vGM model (App. A: Eq. A2), and soil textural classes, BD, θ_{33}, and θ_{PWP} as input parameters for the ROSETTA pedotransfer function. These parameters (Table 3), together with the volumetric SWC at field capacity (θ_{FC}, h = −6 kPa), which is required for model calibration (Section 2.2.3.), were obtained for each soil texture from different data: Soil physical properties derived from disturbed and undisturbed soil samples (Wenzel et al., 2025), and the "Bodenkundliche Kartieranleitung KA6" (German Soil Survey Guideline; Hartmann et al., 2024) were combined with the freely available "SoilGrids250m"[2]; data sets (https://www.soilgrids.org, Version 2, latest access: 30 November 2024; Poggio et al., 2021). Prior to the parameterization of HYDRUS-1D, all necessary soil properties (Fig. 3) were bilinearly disaggregated to a spatial resolution of 70 m (mean Root Mean Square Error (RMSE) = 0.053, mean absolute error (MAE) = 0.045, mean coefficient of determination (R^2) = 0.978, mean bias = -1.5×10^{-4}), in accordance with the desired spatial resolution of the soil water balance simulations. A bilinear disaggregation of spatially distributed input parameters was chosen as it avoids unrealistic extreme values between data points that can occur with cubic or nearest neighbor disaggregation.

Spatially distributed daily meteorological data (German Meteorological Service, 2024), including minimum, average, and maximum air temperature, precipitation, air pressure, relative humidity, and wind speed, were used for specifying atmospheric boundary conditions in each 1D soil column (Fig. 3). These data sets are available for the DEMMIN study area at a spatial resolution of 250 m (Spengler et al., 2021). Prior to analysis, all meteorological data were bilinearly disaggregated to a spatial resolution of 70 m ($RMSE_{mean} = 0.044$, $MAE_{mean} = 0.010$, $R^2_{mean} = 0.995$, mean bias = -4.5×10^{-5}), according to the desired spatial resolution of the soil water balance simulations. The daily sum of precipitation and the respective value of I_{gross} are used to define the time-variable boundary conditions in each 1D soil column.

In HYDRUS-1D, ET_0 is first estimated based on the FAO-56 Penman-Monteith method (App. A: Eq. A3). Potential transpiration (T_P; App. A: Eq. A4) and potential soil evaporation (E_P; App. A: Eq. A5) are then estimated based on the leaf area index (LAI). NASA's 8-Day MODIS LAI product (Level 4) at a spatial resolution of 500 m (Myneni et al., 2002) was used for spatially distributed LAI information. MODIS LAI data are considered consistent for different crops and across spatio-temporal scales (Fritsch et al., 2012). Small-scale discrepancies may be attributed to the impact of input reflectance, retrieval algorithms and the use of a-priori information (Myneni et al., 2002). Nonetheless, MODIS LAI data are advantageous for the use in consecutive simulations due to regular (8-day) observations and the use of the best available observation within this 8-day period to reduce the impact of cloud coverage, compared to other RS LAI products (e.g., Landsat8/9, Sentinel-2). For both simulation periods (1st April to 30th September) in 2021 and 2022, 28 MODIS LAI data sets were obtained from the USGS "EarthExplorer" (https://earthexplorer.usgs.gov/). Prior to analysis, all MODIS LAI data between observation dates were linearly interpolated to derive daily LAI values for each pixel and then bilinearly disaggregated to a spatial resolution of 70 m ($RMSE_{mean} = 0.089$, $MAE_{mean} = 0.076$, $R^2_{mean} = 0.944$, mean bias = 7.2×10^{-4}), according to the desired spatial resolution of the soil water balance simulations (Fig. 3).

[2] The "SoilGrids250m" result from a global soil mapping project, that provides depth-specific (0 cm to 5 cm, 5 cm to 15 cm, 15 cm to 30 cm, 30 cm to 60 cm, 60 cm to 100 cm) soil properties at a spatial resolution of 250 m by fitting an ensemble of machine-learning methods based on about 150,000 soil profiles and 158 soil covariates. The "SoilGrids250m" data sets in each soil layer were in good agreement ($R^2_{mean} = 0.679$, $p < 0.001$) with soil physical properties derived from laboratory analyses of disturbed (for soil textural classes) and undisturbed (for BD) soil samples, which were collected at different depths (10 cm, 20 cm, 30 cm, 50 cm) from two loamy sand and sand potato fields in 2021 and 2022.

Table 3
Depth-specific (0 cm to 10 cm, 10 cm to 20 cm, 20 cm to 30 cm, 30 cm to 60 cm, 60 cm to 100 cm) soil properties (sand content in %; silt content in %; clay content in %; dry bulk density, BD, in g cm^{-3}; saturated hydraulic conductivity, K_{Sat}, in cm d^{-1}; soil water content at saturation, θ_{Sat}, in m^3 m^{-3}; soil water content at field capacity, θ_{FC}, in m^3 m^{-3}; soil water content at h = −33 kPa, θ_{33}, in m^3 m^{-3}; and soil water content at permanent wilting point, θ_{PWP}, in m^3 m^{-3}) per soil texture (sand, loamy sand, sandy loam, sandy clay loam, loam), according to "SoilGrids250m" (Version 2; Poggio et al., 2021). The empirical van-Genuchten-Mualem parameters (residual soil water content, θ_r, in m^3 m^{-3}; α in L^{-1}; n) were derived from the ROSETTA pedotransfer function.

Soil texture	Depth (cm)	Sand (%)	Silt (%)	Clay (%)	BD (g cm^{-3})	K_{Sat} (cm d^{-1})	θ_{Sat} (m^3 m^{-3})	θ_{FC} (m^3 m^{-3})	θ_{33} (m^3 m^{-3})	θ_{PWP} (m^3 m^{-3})	θ_r (m^3 m^{-3})	α (L^{-1})	n (-)
Sand	0–10	86.4	7.8	5.8	1.371	162.3	0.421	0.245	0.161	0.066	0.027	0.0136	1.372
	10–20	87.1	6.7	6.2	1.403	164.9	0.420	0.243	0.162	0.068	0.028	0.0135	1.423
	20–30	89.2	5.6	5.2	1.319	170.1	0.419	0.252	0.170	0.073	0.029	0.0135	1.483
	30–60	86.8	8.5	4.7	1.355	163.6	0.415	0.253	0.171	0.074	0.030	0.0135	1.492
	60–100	91.4	4.4	4.2	1.323	201.5	0.415	0.237	0.140	0.054	0.024	0.0132	1.519
Loamy sand	0–10	77.6	12.2	10.2	1.413	141.9	0.402	0.232	0.153	0.073	0.029	0.0135	1.438
	10–20	78.8	9.9	11.3	1.402	134.2	0.403	0.235	0.153	0.071	0.028	0.0136	1.479
	20–30	78.9	10.1	11.0	1.401	144.8	0.403	0.240	0.153	0.068	0.027	0.0137	1.550
	30–60	80.4	8.7	10.9	1.368	150.4	0.403	0.242	0.158	0.070	0.028	0.0137	1.571
	60–100	81.7	7.5	10.8	1.376	161.6	0.401	0.220	0.146	0.057	0.025	0.0134	1.482
Sandy loam	0–10	62.9	19.7	17.4	1.434	114.2	0.410	0.275	0.179	0.085	0.026	0.0132	1.409
	10–20	63.4	19.5	17.1	1.422	118.3	0.412	0.277	0.183	0.083	0.029	0.0130	1.471
	20–30	64.8	18.9	16.3	1.436	122.2	0.416	0.282	0.188	0.082	0.031	0.0129	1.554
	30–60	67.7	17.0	15.3	1.439	127.4	0.408	0.284	0.188	0.082	0.031	0.0130	1.565
	60–100	68.9	15.9	15.2	1.463	130.3	0.408	0.282	0.186	0.087	0.025	0.0135	1.434
Sandy clay loam	0–10	60.9	14.9	22.2	1.478	75.4	0.417	0.298	0.203	0.093	0.036	0.0127	1.505
	10–20	61.5	14.5	24.0	1.455	80.8	0.415	0.295	0.203	0.090	0.034	0.0127	1.552
	20–30	62.4	14.4	23.2	1.453	85.3	0.414	0.294	0.202	0.085	0.031	0.0127	1.600
	30–60	66.1	12.9	21.0	1.433	88.4	0.414	0.295	0.202	0.085	0.031	0.0127	1.600
	60–100	70.8	9.0	20.2	1.425	95.5	0.396	0.296	0.194	0.079	0.025	0.0134	1.427
Loam	0–10	54.2	30.7	15.1	1.527	64.8	0.402	0.306	0.248	0.120	0.038	0.0130	1.437
	10–20	55.4	30.3	14.3	1.511	66.0	0.400	0.303	0.242	0.115	0.037	0.0129	1.423
	20–30	55.8	30.5	13.7	1.515	70.1	0.400	0.301	0.242	0.113	0.033	0.0128	1.513
	30–60	57.8	28.9	13.3	1.490	73.1	0.397	0.301	0.242	0.113	0.033	0.0128	1.514
	60–100	58.6	28.5	12.9	1.484	75.4	0.395	0.292	0.233	0.109	0.029	0.0131	1.480

The estimated T_P and E_P are then used in conjunction with a crop-specific water stress response (Feddes et al., 1978) and root growth distribution to estimate actual plant transpiration (T_a; App. A: Eq. A6) and soil evaporation (E_a; App. A: Eq. A7). To ensure an accurate simulation of the depth-specific root growth distribution, the maximum rooting depth of each crop was set to the respective value listed in Table 1. However, it should be noted that the soil water balance was only simulated up to a depth of 100 cm, since the root length density of each crop appears to exponentially decrease with increasing soil depth. It is assumed that root water uptake rates decrease in each 1D soil column with water stress, as described by Feddes et al. (1978); App. A: Eq. A8). The required pressure heads are available for all crops analyzed in this study (Table 1) based on the work of Wesseling et al. (1991). To ensure an easy application of the proposed approach, the same pressure heads according to Wesseling et al. (1991) are used for different cultivar varieties of the crops cultivated on the farm.

2.2.3. Calibration and validation

The soil water balance simulations were calibrated for each 1D soil column using the HYDRUS-1D inverse model solution (Fig. 3), which is a promising approach for estimating soil hydraulic properties across spatial scales (Vrugt et al., 2008). The objective of this inverse model solution is to fit the a-priori unknown vGM parameters (α, n, and θ_r), which had previously been estimated for each soil layer using the ROSETTA pedotransfer function (cp. Section 2.2.2.), to other soil physical properties determined in the laboratory. The implemented Levenberg-Marquardt algorithm for parameter optimization (Marquardt, 1963) was used for the inverse solution. Soil layer specific θ_{FC}, θ_{PWP}, and K_{Sat}, (cp. Section 2.2.2.) were used as fitting parameters. All inverse solutions were performed individually for each of the three a-priori unknown vGM parameters. No parameter weighting has been used during the inverse solution, with weighting coefficients set to 1. The use of spatially distributed fluxes at the atmospheric (i.e., ET_C) or lower boundary could allow for higher accuracy of input parameters and associated simulations across spatial scales but was rejected in this study, because direct measurements are not available for either fluxes in each 1D soil column.

The soil water balance simulations were validated in different depths (0 cm to 60 cm, in 10 cm increments), using in-situ SWC measured on a homogeneous loamy sand in 2021 and another loamy sand and sand in 2022. Potatoes were grown on both fields. Both sites were variably irrigated in experimental plots (see Wenzel et al., 2025, for a detailed description). The measurements were conducted from May to September in each year in triplicate per experimental plot (App. B) using 60 cm Sentek drill & drop profile probes (Sentek Sensor Technologies, Stepney, Australia). A total of 12 (18) 1D soil columns from HYDRUS-1D simulations were equipped with measurement devices and used for validation in 2021 (2022). The RMSE (m^3 m^{-3}; Eq. 3), the m^3 m^{-3}; MAE (Eq. 4), and the R^2 (Eq. 5) between simulated and in-situ SWC were calculated for validation:

$$RMSE = \sqrt{\frac{\sum_{i=1}^{n}\left(\theta_i^S - \theta_i^o\right)^2}{n}} \quad (3)$$

$$MAE = \frac{\sum_{i=1}^{n}\left|\theta_i^S - \theta_i^o\right|}{n} \quad (4)$$

$$R^2 = 1 - \frac{\sum_{i=1}^{n}\left(\theta_i^o - \theta_i^S\right)^2}{\sum_{i=1}^{n}\left(\theta_i^o - \overline{\theta_i^o}\right)^2} \quad (5)$$

where n is the number of observations, θ_i^S is the simulated SWC at time step i, θ_i^o is the observed SWC at time step i, and $\overline{\theta_i^o}$ is the mean value of in-situ SWC.

In addition to RMSE, MAE and R^2, the bias (m^3 m^{-3}; Eq. 6) was calculated to examine systematic over- or underestimations of simulated SWC from in-situ SWC:

$$bias = \frac{1}{n}\sum_{i=1}^{n}(\Theta_i^S - \Theta_i^o) \quad (6)$$

where n is the number of observations, Θ_i^S is the simulated SWC at time step i, and Θ_i^o is the observed SWC at time step i. Positive values of the bias indicate a systematic simulation overestimation, while negative values indicate a systematic simulation underestimation.

2.3. Agreement between simulated and remotely-sensed soil water content

The simulated dynamics of SWC (hereinafter referred to as HYDRUS-1D-SWC) were compared in this study with two freely available surface (~0 cm to 5 cm) RS-SWC data sets. Firstly, the SMAP-1km data (Lakshmi and Fang, 2023) are a downscaled SWC product derived from the relationship between SWC and temperature differences (Fang et al., 2022). It is based on a combination of the surface (~0 cm - 5 cm) SMAP-SWC data, provided globally every three hours at a low spatial resolution of 36 km (Reichle et al., 2019), with NASA's "Moderate Resolution Imaging Spectroradiometers" (MODIS) Aqua data. Secondly, S1-SWC data are SWC information derived from "Synthetic Aperture Radar" (SAR) data based on eliminating the need for synchronous roughness observations and assuming short-term constant vegetation and roughness effects on SAR backscatter coefficients (Fan et al., 2025a, b).

Daily SMAP-1km data sets from 1st April to 30th September were obtained from the "National Snow and Ice Data Center" (https://nsidc.org/data/nsidc-0779/versions/1). Note that the SMAP-1km data in 2022 are only available until 29th September, since the underlying data production and provision ceased on this date (Fang et al., 2022). Secondly, S1-SWC data sets at a spatial resolution of 1 km (Fan et al., 2025a) were obtained from the "Pangaea" data repository (https://doi.pangaea.de/10.1594/PANGAEA.968754; Fan et al., 2025b). These data are available at specific overpass dates of the Sentinel-1 satellites during each growing season 2021 and 2022. A total of 59 (24) data sets are available for the study region in 2021 (2022). Note that fewer data are available in 2022 since the Sentinel-1B satellite has not been transmitting any data since 23rd December 2021 (European Space Agency, 2022). The SMAP-1km and S1-SWC data were selected in this study due to their free availability, ease of use and independence from further data processing requirements.

All surface RS-SWC data sets were clipped to the study area ($N_{pixel,\ SMAP\text{-}1km} = 56$; $N_{pixel,S1\text{-}SWC} = 68$). In-situ SWC at 10 cm depth (cp. Section 2.2.3.) was used for validation. A total of 3 pixels of SMAP-1km and S1-SWC were equipped with measurement devices. The RMSE ($m^3\ m^{-3}$; Eq. 3), MAE ($m^3\ m^{-3}$; Eq. 4), R^2 (Eq. 5) and the bias ($m^3\ m^{-3}$; Eq. 6) between RS-SWC and in-situ SWC data sets were calculated for validation. The RMSE, MAE, R^2 and the bias were furthermore calculated between RS-SWC and HYDRUS-1D-SWC at 10 cm depth, for comparison. For this purpose, the simulated HYDRUS-1D-SWC data were spatially aggregated to the spatial resolution of 1 km of the RS-SWC data sets. Note that the comparison between SMAP-1km and S1-SWC, respectively, in-situ SWC and HYDRUS-1D-SWC, was only conducted at the uppermost 10 cm depth, as solely the surface SWC (~0 cm to 5 cm) is represented by the two RS-SWC data sets used in this study.

2.4. Irrigation performance assessment

The spatially distributed irrigation efficiency and potential farm-scale water savings were estimated as potential application examples of spatially distributed HYDRUS-1D simulations for an assessment of the performance of the utilized irrigation technique.

Firstly, the irrigation efficiency was estimated for each irrigated crop (potatoes, wheat, and rye in both growing seasons and sugar beet in 2022; Table 1) as the ratio of the sum of irrigation water that is beneficially used (I_{used}) to I_{gross} (Rochester, 2017). The irrigation efficiency must therefore be distinguished from other commonly used "efficiency metrices", such as the "water use efficiency" (ratio of yield to I_{gross}), or the technical-related "application efficiency" (ratio of water stored within the root-zone of a crop). Furthermore, there are different approaches to define I_{used} among the various disciplines of irrigation research (Table 4; e.g., agricultural, engineering, environmental) and the different agronomic objectives of irrigation (e.g., maximizing yield and quality, optimizing the nutrient use efficiency, minimizing the amount of non-beneficially used water, improving or maintaining the soil productivity). For example, Burt et al. (1997) and Tolk et al. (1995), among others, suggest a clear distinction between the amount of water used for crop transpiration (i.e., T_a) and the amount of water removed from the soil by soil evaporation (E_a). With the objective of adjusting I_{gross} to the actual crop water consumption, defining I_{used} as the sum of T_a could be considered the most rational approach, which is also in line with the estimation of biomass production in the FAO crop-water-productivity model (Raes et al., 2023).

In this study, the irrigation efficiency based on determining I_{used} as crop water consumption by T_a (IE_{Ta}) was hence determined for each 1D soil column (Section 2.2.) as:

$$IE_{Ta} = \frac{\sum T_a}{I_{gross}} \quad (7)$$

where T_a is the crop water consumption by crop transpiration and I_{gross} is the location-specific gross irrigation depth. Accordingly, I_{used} was determined as the sum of T_a between the first and the last irrigation events, which is obtained for each 1D soil column from HYDRUS-1D simulations. Location-specific values of I_{gross} are derived from 7-min GPS-based speed and operating pressure data (Section 2.1.). Precipitation occurring during the irrigation period and related changes in crop water consumption are included in the irrigation efficiency estimations by simulating T_a with HYDRUS-1D. The irrigation efficiency of each 1D soil column was averaged for each crop by averaging IE_{Ta} for the respective area used for cultivating each crop (Table 1).

For comparison, the crop-specific irrigation efficiency based on defining I_{used} as ET_C was determined as:

$$IE_{ETC} = \frac{\sum ET_C}{I_{gross}} \quad (8)$$

Table 4
Overview of main approaches for defining the sum of irrigation water that is beneficially used (I_{used}) by the crop as the numerator in irrigation efficiency equations. T_a: crop transpiration; ET_C: crop evapotranspiration; V_{plant}: Amount of water that ends in harvested plant tissues; R: runoff; DP: deep percolation. It should be noted that other terms of beneficial water uses also include water applied for improving or maintaining soil productivity (e.g., nutrient removal), climate control (e.g., cooling or frost protection of plants), seedbed preparation, or germination (Burt et al., 1997).

Definition of I_{used}	Description	Equation	Reference
Crop water consumption	Water that is extracted from the soil by root water uptake (crop transpiration)	$I_{used} = T_a$	(Burt et al., 1997; Tolk et al., 1995)
Atmospheric water use	Water that is extracted from the soil by atmospheric conditions (crop evapotranspiration)	$I_{used} = ET_c$	(Bos and Wolters, 1990)
Consumptive use	Water that is extracted from the soil by atmospheric conditions and ends in harvested plant tissues	$I_{used} = ET_c + V_{plant}$	(Jensen et al., 1967)
Nonconsumptive use	Water that is extracted from the soil by atmospheric conditions and end in harvested plant tissues and leaves the selected area of consideration	$I_{used} = ET_c + V_{plant} + R + DP$	(Rogers, 1997)

where ET_C is the sum of crop evapotranspiration, i.e., the seasonal sum of water extracted from soil by atmospheric conditions and I_{gross} is the location-specific gross irrigation depth.

Secondly, potential farm-scale water savings are estimated by calculating soil depth-specific surpluses or deficits of SWC, separately for each day of the growing season and in comparison to growth stage specific optimum PAW ranges (Table 1). The surpluses or deficits are expressed in mm per 10 cm soil depth by converting PAW to SWC:

$$SWC = \theta_{PWP} + (\%PAW^* \quad \theta_{FC}) \tag{9}$$

where SWC is the volumetric SWC (mm dm^{-1}), θ_{PWP} is the volumetric SWC at permanent wilting point, %PAW is the plant available water content, and θ_{FC} is the SWC at field capacity.

The surpluses or deficits per 10 cm soil depth were summarized per 1D soil column for all soil depths up to the time-variable maximum rooting depth of each crop (Table 1). A depth-specific estimation of surpluses or deficits enables the consideration of deficits in deeper soil layers due to infiltration and a delayed water supply to the root-zone by leaf interception. Subsequently, all absolute deviations per 1D soil column were summarized for the growing season (1st April to 30th September). The sum of cumulative SWC deviations per crop corresponds to potential seasonal water savings or deficits.

2.5. Statistical analyses

One-way analyses of variance (ANOVA) were performed to identify statistically significant differences between HYDRUS-1D-SWC and in-situ SWC. In addition, ANOVA were performed to identify statistically significant differences between the simulation performance metrices (RMSE, MAE, R^2, mean bias), which were obtained from comparing depth-specific (0 cm to 60 cm depth, in 10 cm increments) HYDRUS-1D-SWC and in-situ SWC. Lastly, ANOVA were performed to identify statistically significant differences between the accuracy metrices (RMSE, MAE, R^2, mean bias), which were obtained from comparing in-situ SWC at 10 cm depth and RS-SWC data sets (SMAP-1km, S1-SWC). In advance, all relevant data sets were tested on normal distribution and variance homogeneity using the Shapiro-Wilk test and the Levene test, respectively. All examined data sets were normally distributed and showed a homogeneous variance, confirming the prerequisites for ANOVA. After each ANOVA, Tukey's honestly significant difference (HSD) test (R-package "agricolae", de Mendiburu, 2023) was applied to determine significant differences in group means at $p \leq 0.05$.

3. Results

3.1. Soil water balance simulations

The average HYDRUS-1D-SWC in the root-zone (0 cm to 60 cm) ranged between 0.038 $m^3\ m^{-3}$ and 0.378 $m^3\ m^{-3}$ in 2021 and between 0.039 $m^3\ m^{-3}$ and 0.372 $m^3\ m^{-3}$ in 2022, respectively. Strong spatial variances occurred in HYDRUS-1D-SWC (Fig. 4, App. C-F), due to spatially varying soil physical properties, meteorological conditions, location-specific values of I_{gross} and the phenological development. The average SWC in the root-zone partly exceeded θ_{FC} during the irrigation period, which lead to unproductive water losses by deep percolation. On the other hand, irrigation was sufficient to maintain the SWC in the soil profile above θ_{PWP} (Fig. 4). The average root-zone HYDRUS-1D-SWC differed from in-situ SWC in both years, although the differences were not significant in 2021 (Table 5). These differences are mainly due to the natural effects of local environmental factors such as topography, soil properties, meteorological conditions and phenological characteristics on the soil water balance (Ehrhardt et al., 2025). In topsoil (0 cm to

Table 5
Average in-situ and simulated (HYDRUS-1D) soil water content (SWC) at different depths (0 cm to 60 cm, in 10 cm increments). Measurements were conducted from 5th May (10th May) to 16th September (2nd September) 2021 (2022) on two irrigated potato fields. The simulated SWC are shown as average values for the pixels equipped with measurement devices (2021: $N_{2021} = 12$, $N_{2022} = 18$). Different lower case letters indicate statistically significant differences between in-situ and simulated SWC, which were identified using one-way analysis of variance (ANOVA) and Tukey's honestly significant difference (HSD) test at $p \leq 0.05$. Additional statistical results (df = residual degrees of freedom, F = F ratios, p = P value of the significance test, RSE = residual standard error) are shown for each ANOVA.

	Soil depth (cm)	In-situ ($m^3\ m^{-3}$)	HYDRUS-1D ($m^3\ m^{-3}$)	F	p	RSE
2021	10	0.108 a	0.101 a	3.52	0.062	0.032
	20	0.139 a	0.132 b	9.84	< 0.001	0.027
	30	0.179 a	0.175 a	1.31	0.253	0.035
	40	0.181 a	0.171 b	7.81	0.006	0.235
	50	0.156 a	0.152 a	3.74	< 0.001	0.024
	60	0.161 a	0.154 b	15.88	< 0.001	0.077
	0–60	0.154 a	0.148 b	6.07	0.023	0.021
2022	10	0.143 a	0.133 b	10.43	0.001	0.022
	20	0.127 a	0.122 b	6.30	0.013	0.014
	30	0.156 a	0.154 a	1.25	0.264	0.015
	40	0.154 a	0.139 b	29.60	< 0.001	0.022
	50	0.151 a	0.147 a	6.59	< 0.001	0.016
	60	0.166 a	0.164 a	2.94	0.048	0.013
	0–60	0.150 a	0.144 a	8.81	< 0.001	0.013

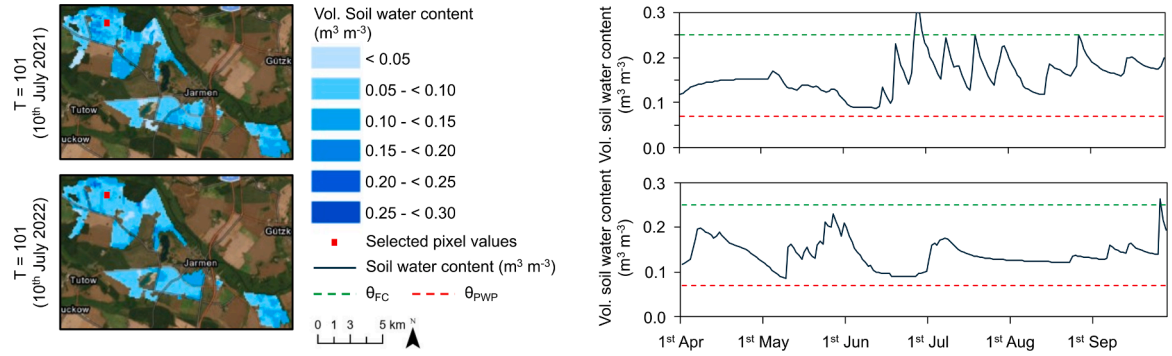

Fig. 4. Simulated farm-scale soil water content ($m^3\ m^{-3}$) in the soil profile (0 cm to 60 cm) at after 101 simulation time steps in 2021 and 2022 (each 10th July; left maps). The daily soil water content is derived from soil water balance simulations with HYDRUS-1D at a spatial resolution of 70 m. Daily soil water content during the growing seasons 2021 and 2022 (1st April to 30th September) is shown as an example for one pixel (red dot), with the volumetric soil water content at field capacity (θ_{FC}, green dotted lines) and at permanent wilting point (θ_{PWP}, red dotted lines). The selected pixel was part of a potato field in 2021 and a wheat field in 2022. The potato crop was irrigated six times during June and July 2021 and the wheat crop was irrigated three times during May and June 2022.

30 cm) layers, particularly precipitation, irrigation and evapotranspiration influenced the soil water balance, resulting in nonlinear patterns of SWC and larger deviations of simulated SWC from in-situ SWC (Fig. 5, Table 5, App. C-F).

The HYDRUS-1D simulations were accurate in comparison to in-situ SWC (Fig. 5), with $RMSE_{mean} = 0.020\ m^3\ m^{-3}$, $MAE_{mean} = 0.017\ m^3\ m^{-3}$ $R^2_{mean} = 0.686$, and an average bias of $-0.008\ m^3\ m^{-3}$ (Table 6). In terms of RMSE, the simulations were most accurate at depths of 20 cm, 30 cm and 50 cm in 2021 and at a depth of 60 cm in 2022, with statistically significant differences to other soil depths. With respect to MAE, the most accurate simulation results were found at depths of 30 cm and 40 cm in 2021 and at a depth of 60 cm in 2022. The R^2 was highest at depths of 20 cm, 30 cm and 50 cm in 2021 and at a depth of 60 cm in 2022. The significantly lowest deviation between simulated and measured SWC in terms of the mean bias was observed at a depth of 10 cm in both years. The lowest accuracy in terms of RMSE and MAE occured at a depth of 10 cm in 2021 and at depths of 10 cm and 20 cm in 2022. The R^2 was lowest at 10 cm depth in both years. The significantly highest deviation between simulated and measured SWC in terms of the mean bias was observed at a depth of 40 cm in 2021 and at depths of 30 cm and 40 cm in 2022 (Table 6). A reduced accuracy in topsoil, when compared to deeper soil layers, is mainly due to the dynamic effects precipitation, irrigation and evapotranspiration. The bias indicates a slight overestimation of SWC at the uppermost 10 cm (2021: $bias_{mean} = 0.013\ m^3\ m^{-3}$; 2022: $bias_{mean} = 0.012\ m^3\ m^{-3}$) and a slight underestimation of SWC at all other soil depths (Table 6).

In addition, a lower accuracy of HYDRUS-1D-SWC, when compared to in-situ SWC, occurred at 40 cm depth compared to 30 cm and 50 cm depth in both years (Fig. 5), which was significant in terms of RMSE, R^2 and the mean bias in 2021 and in terms of R^2 in 2022 (Table 6). This lower accuracy is due to the occurrence of stagnic soil layers at 35 cm and 40 cm depth, which were detected on both fields equipped with measurement devices. Significant differences between the two years were also observed for the RMSE at depths of 20 cm and 40 cm to 60 cm, for the MAE at depths of 20 cm and 50 cm to 60 cm, for the R^2 at depths of 10 cm to 20 cm and 60 cm, respectively. No significant differences between the two years were observed for the mean bias. A higher accuracy at the various soil depths was mostly observed in 2022, except for the RMSE, MAE and R^2 at a depth of 20 cm and with regard to the R^2 at a depth of 10 cm (Table 6).

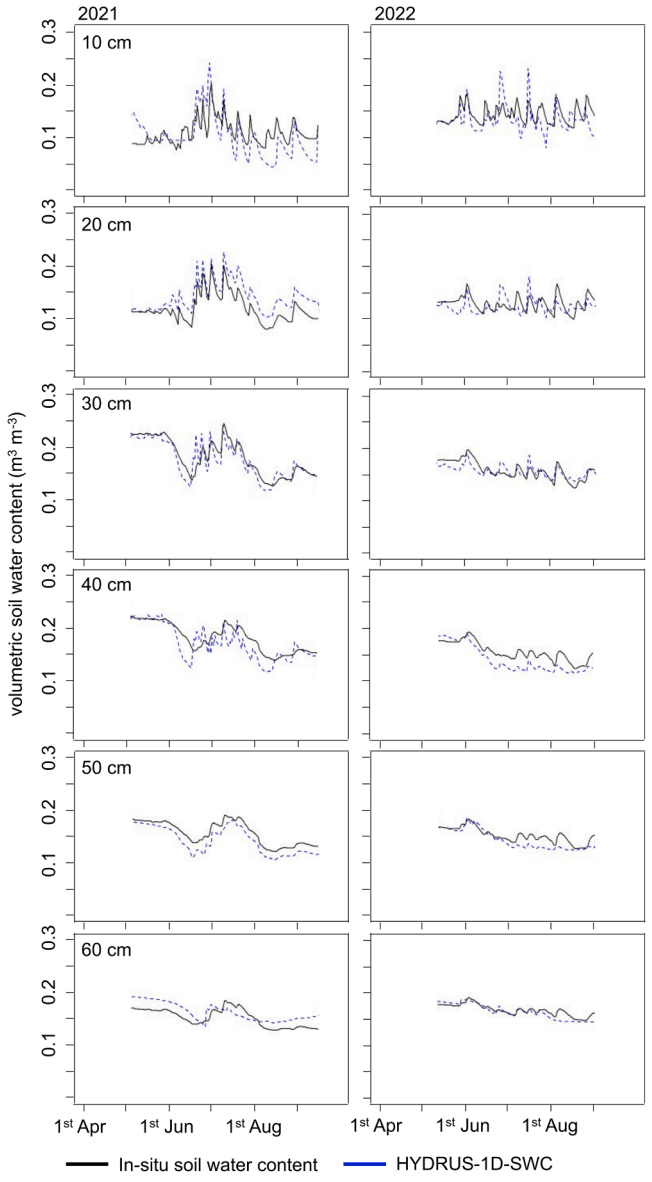

Fig. 5. In-situ (black lines) and simulated (blue dotted lines) soil water content ($m^3\ m^{-3}$) at 0 cm to 60 cm depth, in 10 cm increments. Measurements were conducted from 5th May (10th May) to 16th September (2nd September) 2021 (2022) on two irrigated potato fields. HYDRUS-1D simulations are shown as an example for one pixel each year.

3.2. Agreement between simulated and remotely-sensed soil water content

Both RS-SWC data sets evaluated in this study (SMAP-1km, S1-SWC) provide a moderate representation of surface SWC at a depth from 0 cm to 5 cm (Fig. 6). The overall average accuracy was $RMSE_{mean} = 0.054\ m^3\ m^{-3}$, $MAE_{mean} = 0.046\ m^3\ m^{-3}$, $R^2_{mean} = 0.376$ and $bias_{mean} = 0.091\ m^3\ m^{-3}$, when compared to in-situ SWC.

Although the average RMSE and MAE were only slightly above the corresponding HYDRUS-1D-SWC values at a depth of 10 cm (Table 6), a low R^2 indicates a poor explanation of natural variances in surface SWC by SMAP-1km data. This is particularly evident from stronger variations in the dynamics of surface SWC during precipitation and irrigation, when compared to in-situ SWC (Fig. 6). Moreover, a $bias_{mean}$ of SMAP-1km of $0.032\ m^3\ m^{-3}$ (Fig. 6) indicates a slight overestimation of surface SWC, when compared to in-situ SWC. In general, the accuracy of SMAP-1km, when compared to in-situ SWC, was significantly higher in 2022 than in 2021, with significant differences for all four performance metrices (RMSE, MAE, R^2, bias) between the two years.

When compared to SMAP-1km, S1-SWC showed a less accurate representation of in-situ SWC, with $RMSE_{mean} = 0.075\ m^3\ m^{-3}$ and $MAE_{mean} = 0.062\ m^3\ m^{-3}$ (Fig. 6). Similar to SMAP-1km, a low R^2 ($R^2_{mean} = 0.232$) and bias ($bias_{mean} = 0.142\ m^3\ m^{-3}$) were observed, which indicate a strong overestimation of surface SWC by S1-SWC, when compared to in-situ SWC. Significant differences between S1-SWC and in-situ SWC occured between the two years, with an increased accuracy observed in 2021. These differences are mainly due to the smaller number of available S1-SWC data in 2022 (N = 24), in contrast to 2021 (N = 59).

SMAP-1km agreed only slightly less with HYDRUS-1D-SWC, when compared to in-situ SWC. A better agreement was observed in 2022, when compared to 2021 (Fig. 7). S1-SWC, on the other hand, did not agree well with the HYDRUS-1D-SWC at 10 cm depth, which can particularly be attributed to the different temporal resolution of the two data sets. Both remotely-sensed SWC data sets overestimated the surface SWC, when compared to HYDRUS-1D-SWC, shown by $bias_{mean,SMAP\text{-}1km} = 0.021\ m^3\ m^{-3}$ and $bias_{mean,S1\text{-}SWC} = 0.108\ m^3\ m^{-3}$ (Fig. 7). Whereas the daily resolution of SMAP-1km is more suitable for reproducing temporal dynamics of surface SWC, shown by an increased accuracy, S1-SWC is limited to the specific overpass dates of the Sentinel-1 satellites (~1 week, Fig. 1). S1-SWC must hence be considered less suitable for accurately reproducing the complex dynamic effects of precipitation, irrigation and evapotranspiration on surface SWC.

Table 6
Average simulation performance metrices (Root Mean Square Error, RMSE ($m^3\ m^{-3}$); Mean Absolute Error, MAE ($m^3\ m^{-3}$); coefficient of determination, R^2; mean bias ($m^3\ m^{-3}$)) between in-situ and simulated soil water content at different soil depths (0 cm to 60 cm, in 10 cm increments; A) and years (2021, 2022; B). A total of 12 (18) pixels of spatially distributed soil water balance simulations with HYDRUS-1D were equipped with measurement devices and used for validation. The standard deviation across the different validation pixels is shown for each model performance metric. Different lower case letters indicate statistically significant differences in the model performance metrices between different soil depths within single years, which were identified using one-way analysis of variance (ANOVA) and Tukey's honestly significant difference (HSD) test at $p \leq 0.05$. Different upper case letters indicate statistically significant differences between different years at single soil depths. Additional statistical results (df = residual degrees of freedom, F = F ratios, p = P value of the significance test, RSE = residual standard error) are shown for each ANOVA.

	A: ANOVA for differences between different soil depths within a single year											
				Soil depth (cm)						ANOVA statistics		
B: ANOVA for differences between different years at a single soil depth				**10**	**20**	**30**	**40**	**50**	**60**	**F**	**p**	**RSE**
	Year	**2021**	RMSE ($m^3\ m^{-3}$)	0.038 cA ±0.015	0.022 bA ±0.009	0.015 aA ±0.005	0.020 bB ±0.009	0.016 aB ±0.003	0.015 aB ±0.007	11.45	0.001	0.003
			MAE ($m^3\ m^{-3}$)	0.030 cA ±0.007	0.020 bA ±0.008	0.011 aA ±0.003	0.016 aA ±0.011	0.012 aB ±0.003	0.012 aB ±0.005	10.04	0.001	0.009
			R^2	0.545 cA ±0.089	0.736 aA ±0.107	0.746 aA ±0.043	0.595 bA ±0.079	0.733 aA ±0.050	0.729 aB ±0.045	13.44	0.001	0.089
			mean bias ($m^3\ m^{-3}$)	0.013 aA ±0.002	0.027 cA ±0.019	-0.022 bA ±0.003	-0.046 dA ±0.035	-0.033 cA ±0.024	0.025 cA ±0.017	1.05	< 0.001	0.009
		2022	RMSE ($m^3\ m^{-3}$)	0.039 bA ±0.018	0.031 bB ±0.016	0.011 aA ±0.008	0.015 aA ±0.011	0.010 aA ±0.006	0.009 aA ±0.005	7.13	0.003	0.003
			MAE ($m^3\ m^{-3}$)	0.035 cA ±0.019	0.028 cB ±0.012	0.010 bA ±0.003	0.013 bA ±0.010	0.008 bA ±0.003	0.008 aA ±0.002	3.71	0.001	0.011
			R^2	0.470 eB ±0.101	0.571 dB ±0.099	0.771 bA ±0.065	0.663 cA ±0.080	0.743 bA ±0.045	0.837 aA ±0.027	24.43	0.001	0.103
			mean bias ($m^3\ m^{-3}$)	0.012 aA ±0.007	-0.021 bA ±0.014	-0.018 bA ±0.006	-0.038 cA ±0.033	-0.031 cA ±0.019	-0.024 bA ±0.008	0.04	< 0.001	0.010
	ANOVA statistics	**F**	RMSE	2.43	5.21	3.82	1.89	3.29	5.95			
			MAE	2.39	5.51	3.30	1.74	3.21	6.09			
			R^2	5.75	15.2	25.05	18.44	44.89	33.35			
			mean bias	1.37	7.25	6.01	3.29	7.18	1.07			
		p	RMSE	< 0.001	< 0.001	< 0.001	0.003	< 0.001	0.002			
			MAE	0.002	< 0.001	< 0.001	0.004	0.003	< 0.001			
			R^2	0.003	< 0.001	< 0.001	0.002	< 0.001	0.001			
			mean bias	< 0.001	< 0.001	< 0.001	< 0.001	< 0.001	< 0.001			
		RSE	RMSE	0.008	0.009	0.010	0.009	0.009	0.010			
			MAE	0.011	0.010	0.010	0.014	0.010	0.007			
			R^2	0.072	0.103	0.029	0.056	0.014	0.087			
			mean bias	0.010	0.045	0.015	0.031	0.065	0.038			

The overall lower agreement between HYDRUS-1D-SWC and surface RS-SWC data sets, when compared to the accuracy between HYDRUS-1D-SWC and in-situ SWC, can be attributed to the differences in the soil depths, which are reflected by the different data sets. Whereas RS-SWC is basically limited to soil depths of ~0 cm to 5 cm, a depth of 10 cm is reflected by both in-situ SWC and HYDRUS-1D-SWC. These differences in the respective soil depth particularly explain low R^2 between SMAP-1km and S1-SWC, compared to in-situ SWC and HYDRUS-1D-SWC. Additionally, HYDRUS-1D-SWC was spatially aggregated to a spatial resolution of 1 km, in order to achieve the spatial resolution of SMAP-1km and S1-SWC. This spatial aggregation could potentially have led to information losses, which could have resulted in a reduced agreement between SWC obtained from HYDRUS-1D-SWC and remotely-sensed SWC, compared to in-situ SWC.

3.3. Irrigation performance assessment

3.3.1. Irrigation efficiency

The average farm-scale IE_{Ta} was 59.5 % in 2021 and 56.7 % in 2022 (Fig. 8). Large variations in IE_{Ta} were observed among the various crops, which particularly emphasize the need for considering differences in the phenological characteristics between different crops. In general, the crop-specific IE_{Ta} was higher in 2021 than in 2022, which is mainly due to higher crop-specific values of I_{gross} in 2022 (Table 1). Cereals (wheat, rye) showed considerably lower IE_{Ta} values, when compared to tuber crops (potato, sugar beet). These differences are attributed to higher LAI values of tuber crops and lower root water uptake rates of cereals during their advanced phenological development, which are used in HYDRUS-1D for simulating the crop water consumption (i.e., T_a; Eq. A4, A6).

Using ET_C instead of T_a resulted in an increased irrigation efficiency among the various crops (App. G). The differences between both

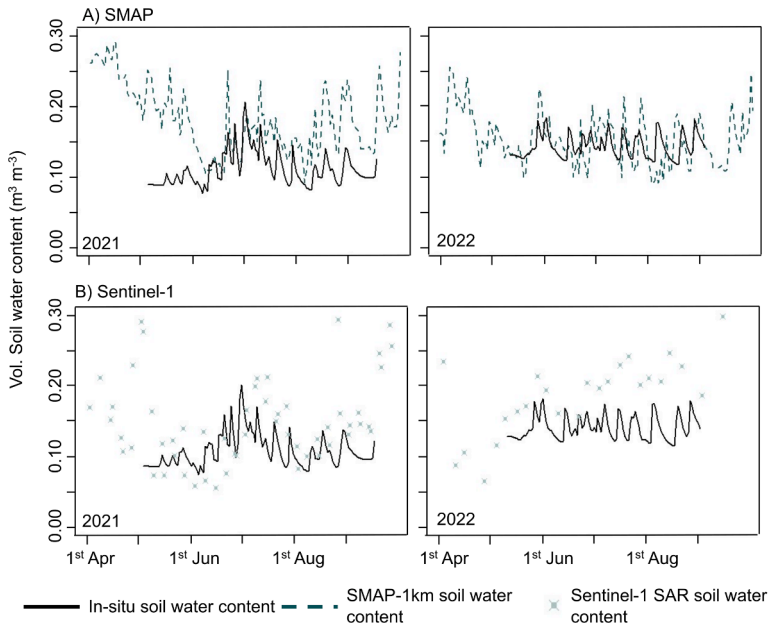

			SMAP-1km	S1-SWC
Year	2021	RMSE ($m^3 m^{-3}$)	0.066 b ±0.026	0.060 a ±0.029
		MAE ($m^3 m^{-3}$)	0.055 b ±0.015	0.044 a ±0.023
		R^2	0.301 b ±0.075	0.289 a ±0.056
		mean bias ($m^3 m^{-3}$)	0.062 b ±0.046	0.127 a ±0.071
	2022	RMSE ($m^3 m^{-3}$)	0.041 a ±0.015	0.089 b ±0.024
		MAE ($m^3 m^{-3}$)	0.036 a ±0.013	0.079 b ±0.024
		R^2	0.450 a ±0.055	0.174 b ±0.041
		mean bias ($m^3 m^{-3}$)	0.017 a ±0.008	0.157 b ±0.063
ANOVA statistics	F	RMSE	2.15	5.33
		MAE	1.34	4.01
		R^2	58.78	93.40
		mean bias	3.13	4.79
	p	RMSE	<0.001	<0.001
		MAE	<0.001	<0.001
		R^2	<0.001	<0.001
		mean bias	<0.001	<0.001
	RSE	RMSE	0.008	0.026
		MAE	0.014	0.035
		R^2	0.065	0.032
		mean bias	0.023	0.101

Fig. 6. Soil water content (m^3 m^{-3}) during the growing seasons (1st April to 30th September) 2021 (left) and 2022 (right) at 10 cm depth provided by in-situ measurements (black lines) on two variably irrigated potato fields, the downscaled "Soil Moisture Active and Passive" (SMAP-1km) soil water content (A, top row; green dotted lines; Fang et al., 2022), and the Sentinel-1 (S1-SWC) soil water content derived from Synthetic Aperture Radar (SAR) sensors (B, bottom row; red points; Fan et al., 2025a, b). Remotely-sensed surface soil water content is shown for one pixel, which was equipped with measurement devices. The overall average statistical accuracy metrices (Root Mean Square Error, RMSE (m^3 m^{-3}); Mean Absolute Error (m^3 m^{-3}), MAE; coefficient of determination, R^2; mean bias (m^3 m^{-3})), including the standard deviation across all validation pixels, are shown in the table for each year. Lower case letters indicate statistically significant differences in the model performance metrices between the two growing seasons, which were identified using one-way analysis of variance (ANOVA) and Tukey's honestly significant difference (HSD) test at $p \leq 0.05$. Additional statistical results (df = residual degrees of freedom, F = F ratios, p = P value of the significance test, RSE = residual standard error) are shown for each ANOVA. Note that (i) no daily soil water content is available from Sentinel-1 due to orbit duration, and (ii) less data are available in 2022 (N = 24), when compared to 2021 (N = 59) since the Sentinel-1B satellite has not been sending data since 23rd December 2021 (European Space Agency, 2022).

irrigation efficiencies differed between cereals (wheat, rye) and tuber crops (potatoes, sugar beet), due to differences in the above-ground biomass, which resulted in a decreased water withdrawal from the soil by E_a during the irrigated period. The differences between both irrigation efficiencies of tuber crops were moreover higher in 2021 than in 2022, as irrigation was applied more frequently before canopy closure, which resulted in an increased ratio of E_a (App. G).

Additionally, the potato crop was irrigated five times in 2021 and six times in 2022. Higher I_{gross} in 2022 (Table 1) could have led to a decline in the ratio of I_{used} and hence the estimated irrigation efficiency of potatoes in 2022 (Fig. 8). Despite an increase in I_{gross} of 13.8 mm, the irrigation efficiency only decreased by 4.7 % in 2022 compared to 2022, which is particularly due to an increased average air temperature, reduced effective precipitation and thus higher crop water consumption (T_a) in 2022 (Table 2). On the other hand, although I_{gross} of wheat and rye had increased in 2022, substantially higher IE_{Ta} estimates of both wheat and rye were observed in 2022, when compared to 2021 (Fig. 8). These increased IE_{Ta} values for cereals in 2022 indicate that increased values of I_{gross}, which aim to compensate for lower precipitation, were more suitable for compensating for water withdrawal from the soil through water consumption of cereals.

3.3.2. *Farm-scale water savings*

The cumulative seasonal deficits or surpluses of SWC were estimated as the sum of all absolute deviations of SWC in comparison to crop-specific optimum PAW per 1D soil column for the growing season (1st April to 30th September). The deviations ranged from −0.36 m^3 m^{-2} to 2.15 m^3 m^{-2} in 2021 and from −0.42 m^3 m^{-2} to 2.56 m^3 m^{-2} in 2022 (Fig. 9). Such high overall maximum values, however, are particularly due to locally occurring technical faults of the utilized gun sprinkler irrigation systems and thus appear only at occasional locations (Fig. 9). The overall average cumulative deviations of SWC from optimum PAW were 5.4 mm in 2021 and 4.5 mm in 2022. Accordingly, potential farm-scale water savings, i.e., the sum of crop-specific cumulative seasonal deviations of SWC in comparison to optimum PAW per crop, amounted to 87,006.9 m^3 in 2021 and to 71,396.6 m^3 in 2022, for all fields of the farm. These values correspond to the water use of 1000 average households (300 m^3 d^{-1}) for 290 and 238 days, respectively. A lower potential for farm-scale water savings in 2022 compared to 2021 is mainly due to a smaller area under irrigation (Table 1) and higher CWR in 2022 attributed to the meteorological conditions (Table 2).

The seasonal crop-specific surpluses, i.e., potential water savings, were generally lower in 2022 than in 2021, except for wheat. Additionally, seasonal crop-specific deficits, i.e., an SWC below the crop-specific optimum PAW, on average, were higher in 2021 than in 2022 for all crops (Fig. 9). For the irrigated crops (potato, wheat, rye, sugar beet), increased values of I_{gross} in 2022 aimed to compensate for lower precipitation and were sufficient to meet the crop-specific optimum PAW ranges of potatoes, wheat, and sugar beet (Fig. 9). Sugar beet was characterized by a large surplus in 2021, even though these crops were not irrigated in 2021 (Fig. 9). The seasonal deficits only relate to the non-irrigated crops (except rye) and are mainly due to lower precipitation in 2022. The SWC on the non-irrigated rapeseed fields were in line the crop-specific optimum PAW ranges, resulting in a small overall farm-scale seasonal surplus of 1.8 m^3 (Fig. 9).

4. Discussion

4.1. *Soil water balance simulations*

The integration of a-priori information on depth-specific soil physical properties, weather conditions, location-specific values of I_{gross}, and

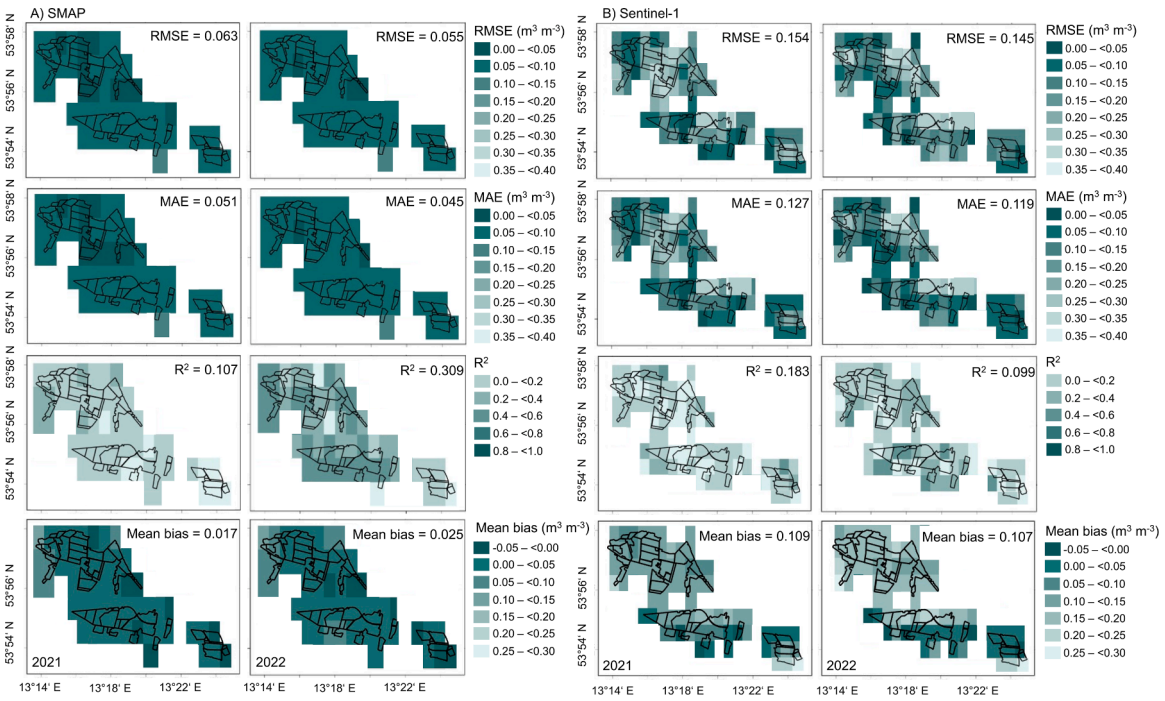

Fig. 7. Spatially distributed agreement (first row: Root Mean Square Error, RMSE ($m^3\ m^{-3}$); second row: Mean Absolute Error, MAE ($m^3\ m^{-3}$); third row: coefficient of determination, R^2; fourth row: mean bias ($m^3\ m^{-3}$)) between HYDRUS-1D simulations at 10 cm depth and the soil water content of the downscaled "Soil Moisture Active and Passive" (SMAP-1km; Fang et al., 2022) product (A, first and second column) and Sentinel-1 (B, third and fourth column; Fan et al., 2025a, b) data in 2021 (left) and 2022 (right). White lines indicate the fields of the farm in Mecklenburg-Western Pomerania, Germany ($N_{pixel,SMAP\text{-}1km} = 56$; $N_{pixel,S1\text{-}SWC} = 68$). The overall farm-scale average values for each of the four metrices are shown in each figure. Note that (i) no daily soil water content is available from Sentinel-1 due to orbit duration, and (ii) less data are available in 2022 (N = 24), when compared to 2021 (N = 59) since the Sentinel-1B satellite has not been sending data since 23rd December 2021 (European Space Agency, 2022).

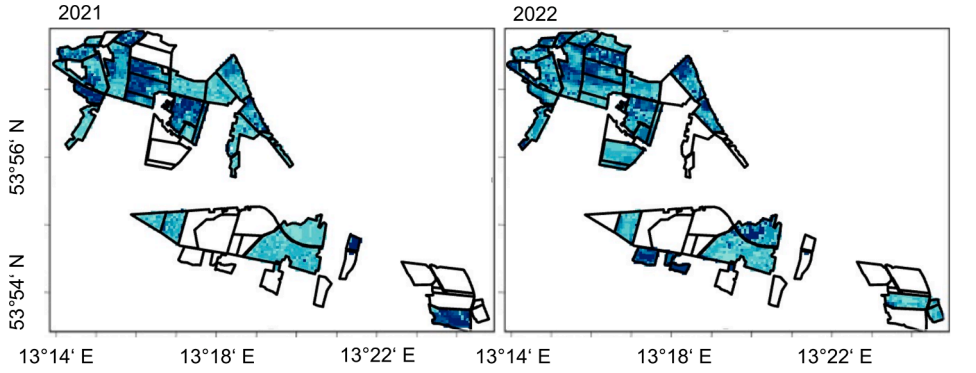

	2021	2022
Potato (%)	67.3	62.6
Wheat (%)	43.9	50.7
Rye (%)	40.3	40.6
Sugar beet (%)	no irrigation	58.2
Average irrigation efficiency (%)	59.5	56.7

Fig. 8. Spatially distributed irrigation efficiency (%) on all irrigated fields as the ratio of the average sum of irrigation water beneficially used by the crop and the gross irrigation depth. The sum of beneficially used irrigation water was defined as the actual transpiration between single irrigation events, which was derived from soil water balance simulations at a spatial resolution of 70 m with HYDRUS-1D from 1st April to 30th September 2021 (left figure) and 2022 (right figure). The overall average irrigation efficiency for each crop are shown in the table below. Non-irrigated crops (2021: barley, rapeseed, sugar beet, lupin; 2022: barley, rapeseed, lupin) are indicated by non-colored fields in both maps.

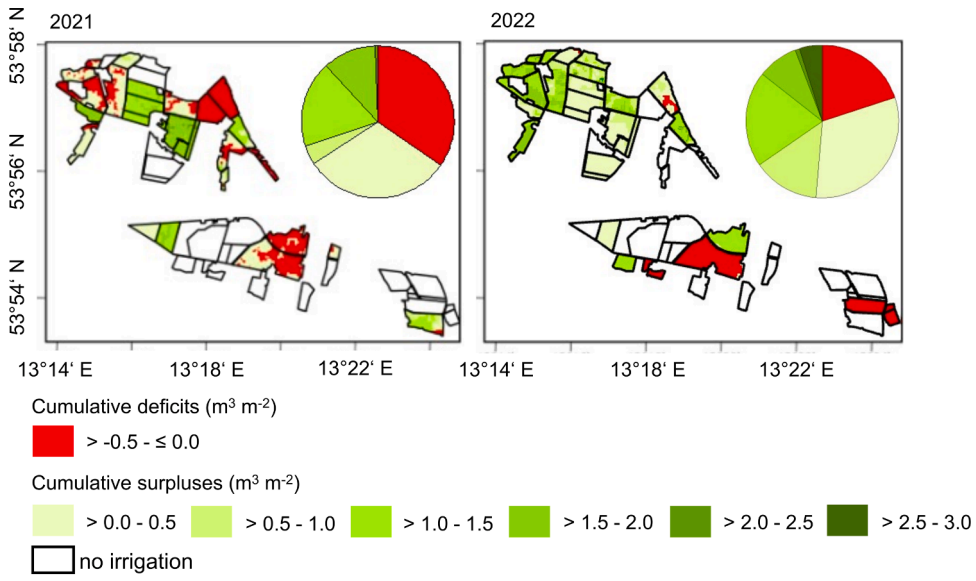

	2021	2022
Potato (m^3)	77,358.60	56,533.19
Wheat (m^3)	6,499.77	12,783.54
Barley (m^3)	-3.81	-22.57
Rye (m^3)	-20.26	-37.39
Rapeseed (m^3)	1.80	-399.09
Sugar beet (m^3)	3305.51	2895.44
Lupin (m^3)	-133.96	-356.48
Sum of seasonal surplus / deficit (m^3)	91,740.92	76,714.72

Fig. 9. Spatially distributed cumulative deficits (red scale) or surpluses (green scale) of the soil water content at 0 cm to 60 cm depth on all irrigated fields, in comparison to crop-specific optimum ranges of plant available water content. Depth-specific (0 cm to 60 cm, in 10 cm increments) soil water content was derived from soil water balance simulations at a spatial resolution of 70 m with HYDRUS-1D from 1st April to 30th September 2021 (left figure) and 2022 (right figure). Pie charts in both maps indicate the distribution of the different classes of deficits and surpluses in the soil water content. The overall cumulative deficits or surpluses for each crop are shown in the table below and were used to estimate potential seasonal and farm-scale water savings. Non-irrigated crops (2021: barley, rapeseed, sugar beet, lupin; 2022: barley, rapeseed, lupin) are indicated by non-colored fields in both maps.

phenological characteristics enabled an application of the HYDRUS-1D software environment in a spatially distributed manner. Different components of the soil water balance (SWC, PAW, ET_C, infiltration, root water uptake) were simulated at daily time steps at a spatial resolution of 70 m x 70 m. The simulations were accurate in comparison to in-situ SWC, which was measured on two loamy sands and a pure sand cultivated with potatoes, with overall average metrices of $RMSE_{mean} = 0.020\ m^3\ m^{-3}$, $MAE_{mean} = 0.017\ m^3\ m^{-3}$, $R^2_{mean} = 0.676$, and a $bias_{mean}$ = -0.008 $m^3\ m^{-3}$. This simulation accuracy is in line with numerous experimental studies for various soil textures and crops. For instance, Kisekka et al., (2022), Kumar et al. (2022), Usman et al. (2025) and Ventrella et al. (2019) reported values of RMSE $\leq 0.020\ m^3\ m^{-3}$, MAE $\leq 0.020\ m^3\ m^{-3}$, $R^2 \geq 0.600$ and a bias between $0.012\ m^3\ m^{-3}$ and $0.036\ m^3\ m^{-3}$ for variably irrigated sites at different environmental conditions.

So far, nonetheless, there have been as yet no studies that report comparable simulation accuracies of spatially distributed HYDRUS-1D simulations across different soil textures and crops. This observed lack of spatially distributed HYDRUS-1D simulations for PI is a direct consequence of trade-offs between the aim of a most precise simulation of the soil water balance while minimizing the required efforts for data processing (Kuznetsov et al., 2012; Lazarovitch et al., 2023; Mao et al., 2021; Rezaei et al., 2017). Here, two-dimensional or three-dimensional models are capable of more accurately simulating the soil water balance across spatio-temporal scales, with respect to spatially heterogeneous environmental factors and their effects on the soil water balance (Costanzo et al., 2024). But the availability, quality and scalability of two-dimensional or three-dimensional model input parameters (particularly depth-specific soil physical properties) and significantly increased computational efforts for data processing, calibration and uncertainty analyses severely limit the applicability of complex simulations with HYDRUS-2D/3D, for instance, in agricultural practice (Gu et al., 2020). This is particularly due to a more precise characterization of the complex water flow processes in the root-zone (Vereecken et al., 2016), shown by significantly improved simulation performance metrices, with reported values of RMSE $\leq 0.017\ m^3\ m^{-3}$, MAE $\leq 0.015\ m^3\ m^{-3}$, $R^2 \geq 0.700$ and a mean bias of $\pm 0.020\ m^3\ m^{-3}$ (e.g., Cordel et al., 2025; Costanzo et al., 2024; Ghazouani et al., 2019; Kandelous and Šimůnek, 2010; Song et al., 2025; Zhao et al., 2024).

4.2. *Agreement between simulated and remotely-sensed soil water content*

Both RS-SWC data sets used in this study (SMAP-1km, S1-SWC) were moderately accurate in terms of RMSE and MAE, when compared to in-situ SWC, but fall short in the agreement in terms of R^2. Additionally, the agreement between HYDRUS-1D-SWC and both RS-SWC data sets was rather low, although SMAP-1km was in better agreement across all fields of the farm than S1-SWC. Both RS-SWC data sets showed an

overestimation of surface SWC, when compared to HYDRUS-1D, which is particularly due to the different soil depth depicted by both approaches (RS-SWC: ~0 cm to 5 cm, HYDRUS-1D-SWC: 10 cm). These results illustrate an increased suitability of HYDRUS-1D soil water balance simulations for mapping the dynamics of surface SWC, when compared to RS data sets.

Both RS-SWC data sets are subject to inherent uncertainties associated with the applied algorithms for deriving SWC information at a spatial resolution of 1 km. The downscaling of the original SMAP product to 1 km improved the spatial resolution of SMAP-SWC but the high resolution data sets used for this purpose (MODIS land surface temperature data) carry their own inherent errors, which propagate into the derived SWC estimates at a spatial resolution of 1 km (Zheng et al., 2023). The values of RMSE found for SMAP-1km data fall short of the expected performance by SMAP mission requirement (unbiased RMSE < 0.04 m^3 m^{-3}; Colliander et al., 2017). Nonetheless, several regional studies (e.g., Ray et al., 2017; Suman et al., 2020) have reported RMSE ≥ 0.050 m^3 m^{-3} for SMAP-1km data, indicating that such deviations are expected and may reflect site specific characteristics and external factors such as precipitation variability and frequent irrigation as observed in this study. In this context, the procedure for downscaling SMAP-SWC to SMAP-1km may not fully capture all variations of SWC (Peng et al., 2021). The accuracy of S1-SWC data is limited to vegetation and surface roughness effects, which can lower the accuracy of the derived SWC, particularly under dense crop cover (Massart et al., 2024). Particularly, vegetation cover often results in an underestimation of SWC and higher errors at field scale due to signal absorption and scattering effects of the vegetation (Balenzano et al., 2021). Accordingly, the error of S1-SWC data is expected to range between RMSE = 0.030 m^3 m^{-3} and RMSE = 0.080 m^3 m^{-3} (El Hajj et al., 2017; Fan et al., 2025). The RMSE values found in this study for S1-SWC exceed these commonly expected error ranges, particularly attributed to the effects of frequent irrigation and vegetation cover. In this study, the effects of precipitation, evapotranspiration and irrigation on (surface) SWC dynamics were more accurately reproduced by HYDRUS-1D simulations, when compared to the freely available surface RS-SWC data sets. While satellite products are indispensable for large scale SWC monitoring (Mahmood et al., 2024), they often exhibit an increased uncertainty following precipitation and irrigation events due to wet surface scattering which contribute to signal attenuation (Gibon et al., 2024). This limitation is particularly evident in irrigated agricultural areas where changes in SWC changes at fine temporal scales are difficult to capture using satellite observations, requiring higher temporal resolution that aligns with irrigation frequency (Kragh et al., 2024).

The comparison between spatially distributed HYDRUS-1D simulations and satellite derived RS-SWC is limited by both temporal mismatches and depth limitations inherent in existing RS-SWC data sets (e.g., SMAP-1km, S1-SWC). Particularly, S1-SWC data sets provide less frequent observations (~three to seven days), when compared to the daily soil water balance simulations conducted in this study. As a result, a total of 59 (24) S1-SWC data sets are available for the study region in 2021 (2022). SMAP-1km, on the other hand, is also provided a temporal resolution of one day, enhancing the comparability with HYDRUS-1D-SWC data sets. Further limitations concern the availability of only surface RS-SWC for comparison, particularly with respect to the purpose of PI, which requires depth-specific SWC as more important for crop growth (Li et al., 2023). Whereas both SMAP-1km and S1-SWC represent the uppermost ~0 cm to 5 cm, the HYDRUS-1D soil water balance simulations are conducted at a depth of 10 cm. Such discrepancies must be carefully accounted for when integrating or evaluating RS-SWC data with simulated SWC dynamics.

4.3. Irrigation performance assessment

The simulated components of the spatially distributed soil water balance (SWC, PAW, ET_C, infiltration, root water uptake) were used for an in-depth assessment of the performance of the utilized traveling gun sprinkler irrigation system. Due to peculiar irrigation scheduling procedures, technical properties of the utilized irrigation system and location-specific environmental factors (soil properties, meteorological conditions, phenological characteristics), the estimates of IE_{Ta} and the derived potentials for water savings are specific for the investigated fields of an existing farm and comparable to other cropping systems only to a limited extent. Nonetheless, the proposed approach for spatially distributed soil water balance simulations enable an application of both approaches also to other environmental conditions and cropping systems. Moreover, the estimates of both IE_{Ta} and potential farm-scale water savings particularly illustrate the specific advantages of spatially distributed HYDRUS-1D simulations for PI purposes.

4.3.1. Irrigation efficiency

So far, different soil water balance models have been used in numerous studies to estimate the application efficiency, the irrigation water productivity, the water use efficiency, or optimum values of I_{gross} across spatial scales (e.g., Brocca et al., 2018; Kharrou et al., 2021; Wenzel et al., 2025; Zaussinger et al., 2019). Also the irrigation efficiency of gun sprinkler irrigation systems has been estimated in regional studies to range between 65 % and 75 % (Howell, 2003), by the use of root-zone SWC simulations (e.g., Pereira and Marques, 2017; Zhang and Long, 2021). Lower values of IE_{Ta} found in this study (57.6 %, on average) are particularly due to varying concepts of defining I_{used} (Table 4). The common definition of I_{used} as ET_C is considered useful for assessing the irrigation performance for maintaining or improving soil productivity (e.g., salt removal, nutrient management) and controlling microclimatic effects on crop productivity (Burt et al., 1997). Therefore, it is assumed that ET_C is approximately equal to the actual crop water consumption (i.e., T_a), even before the canopy closure. Nonetheless, defining I_{used} as ET_C lacks a precise characterization of water losses from the soil associated with excessively frequent irrigation events and for irrigation before canopy closure (Tolk et al., 1995). In this context, the water losses by E_a must be considered non-beneficial for crop productivity. Several studies have already reported that a wet soil surface (e.g., during or immediately after irrigation) significantly increases the ratio of E_a, even at a closed canopy (Liebhard et al., 2022). Accordingly, defining I_{used} as T_a is the most reasonable approach to exclude non-beneficially used water removal from the soil. Although the different HYDRUS models (HYDRUS-1D/2D/3D) are advantageous in this context through the partitioning of ET_C in E_a and T_a (Er-Raki et al., 2021), they have to our knowledge so far not been used for spatially distributed irrigation efficiency estimations, mainly due to the required input parameters and processing efforts. Crop-specific variations in the estimated IE_{Ta} are particularly due to phenological differences between different crops and associated uncertainties inherent in the approach for partitioning of ET_C in E_a and T_a, particularly for high atmospheric demands, large temporal variabilities in crop development or spatial heterogeneities of the canopy cover (Sutanto et al., 2012).

4.3.2. Farm-scale water savings

The estimated potentials for crop-specific water savings correspond to adopted average values of I_{gross} (i.e., with no cumulative surpluses or deficits) of 69.5 mm and 16.1 mm for potatoes and wheat in 2021 and 81.8 mm, 28.6 mm and 14.0 mm for potatoes, wheat and sugar beet in 2022. Uncertainties of the estimated potentials for farm-scale water savings are particularly related to inherent uncertainties of the partitioning of ET_C in E_a and T_a based on LAI-dependent functions in HYDRUS-1D soil water balance simulations. Although inaccurate estimates of ET_C under high atmospheric demands, large temporal variabilities in canopy development, or spatially heterogeneous canopy cover (Sutanto et al., 2012) may propagate into water savings estimations, the impact of short-term ET_C errors is considered negligible through the applied temporal aggregation over the growing season. Typically, it is assumed that water savings between 10 % and 40 % can

be obtained with traveling gun sprinkler irrigation systems by the use of precise estimates of location-specific CWR and according spatially varying values of I_{gross} (Pierce, 2010; Sadler et al., 2005), although dependent on the prevailing soil and meteorological conditions and specific crop and cultivar properties. In comparison to the actual values of I_{gross} (Table 1), the adopted values of I_{gross} amount to 88.9 % (potatoes), 88.5 % (wheat) and 83.6 % (sugar beet), on average for both growing seasons. Similar potentials for saving water with optimized irrigation scheduling have already been found in previous studies (Wenzel et al., 2022, 2025) for the same study region by a detailed assessment of the crop water productivity and the technical-related application efficiency for potato irrigation.

This indicated over-irrigation of different crops is particularly attributable to overestimations of location-specific CWR by the farmer and an underestimation of unproductive water losses during irrigation. In this study, the ZEPHYR irrigation decision support system (Michel and Dannowski, 2013) was used by the farmer for irrigation scheduling. Compared to the proposed approach for spatially distributed soil water balance simulations, ZEPHYR offers the following advantages: (i) low data, processing and decision-making effort, (ii) inclusion of current weather forecast information, and (iii) provision of complete irrigation schedule. To simplify application, ZEPHYR (and also other frequently used tools in German irrigated agriculture such as "agrowetter beregnung"; German Meteorological Service, 2017), use simple soil water balance or tipping-bucket models based on crop-specific optimum PAW ranges, which results in a reduced accuracy of soil water balance simulations, when compared to a physically-based description of water flow processes in the root-zone (Wenzel et al., 2025). Furthermore, spatial heterogeneities in soil physical properties, meteorological conditions or the phenological development are not considered in soil water balance simulations. Accordingly, the provided irrigation recommendations are often not suitable in terms of actual CWR for all small-scale heterogeneities. However, in-field specific irrigation recommendations by ZEPHYR are still technically achievable, e.g., via an application to specific sub-units (e.g., pixels) of a field or irrigation management zones.

4.4. Evaluation of the proposed simulation framework

4.4.1. Limitations of spatially distributed soil water balance simulations

The proposed framework for spatially distributed soil water balance simulations with HYDRUS-1D is subject to different limitations, which are required to be critically considered in the context of PI.

Firstly, one-dimensional soil water balance simulations inherently approximates the small-scale complexity of the hydrological system (Vereecken et al., 2016), by neglecting any lateral flows within and between single 1D soil columns and topography-driven redistribution of water in the root-zone of the crop (Kuznetsov et al., 2012; Mao et al., 2021; Šimůnek et al., 2012a, b). Due to a relatively even with an average slope of 1.52°, at least topography-driven effects on the small-scale soil water balance can be neglected for the study area. Still, inaccurate simulation results may occur for locally higher slopes or partially occurring ponding conditions near kettle holes (Fig. 2; Piernicke et al., 2025).

In this context, secondly, a spatial resolution of 70 m, which was chosen in accordance with the average working width of the utilized traveling gun sprinkler irrigation system, generalizes small-scale heterogeneities in soil properties, irrigation uniformity, lower and atmospheric boundary conditions, or groundwater levels – factors known to control the in-field specific variability of the soil water balance as required for PI (Ehrhardt et al., 2025; Haghverdi et al., 2016; Rezaei et al., 2017). A spatial resolution of 30 m, however, which may be required for more precise irrigation techniques such as center pivot irrigation systems, did not show any differences in the simulation performance, when compared to the 70 m resolution.

Thirdly, the vGM parameters derived from the ROSETTA pedotransfer function involve inherent uncertainties due to a limited representativeness of training data for capturing local structural features, macroporosity, hysteretic effects, or extreme wet and dry conditions (Schaap et al., 2001; Vereecken et al., 2010). Although an inverse calibration using the Marquardt-Levenberg parameter optimization procedure reduces these parameter uncertainties, residual biases may persist, particularly near saturation and under dry-end conditions of the soil water retention and hydraulic conductivity functions (Šimunek et al., 2000). Nonetheless, the ROSETTA pedotransfer function is considered as providing accurate estimates of vGM parameters for various soil and meteorological conditions (Vereecken et al., 2010). In this study, moreover, the highest possible amount of input data (soil textural classes, BD, θ_{33}, and θ_{PWP}) was used for the ROSETTA pedotransfer function, yielding accurate estimates of vGM parameters.

Fourthly, the soil layer sequencing (0 cm to 10 cm, 10 cm to 20 cm, 20 cm to 30 cm, 30 cm to 60 cm, 60 cm to 100 cm; Fig. 3) used for soil water balance simulations does not fully cover the maximum rooting depth of cultivated crops (Table 1). However, the root length density of the cultivated crops is considered as ranging between < 0.01 cm cm^{-3} and 0.4 cm cm^{-3} in soil depths below 100 cm, at least for the soil and climate conditions in Central Europe (e.g., Bublitz et al., 2022; Kemper et al., 2022). It is hence assumed that roots located in soil layers below 100 cm are not providing significant contributions to root-water uptake rates, when compared to the uppermost 100 cm.

And fifthly, the HYDRUS-1D partitioning of ET_C in E_a and T_a based on LAI-dependent functions (App. A) is associated with uncertainties affecting ET_C estimates under conditions of high atmospheric demands, large temporal variabilities in canopy development, or spatially heterogeneous canopy cover (Sutanto et al., 2012). Nonetheless, this approach was chosen in this study as it provides valuable information on the different components of ET_C, which are required for an irrigation performance assessment, e.g., by estimating the irrigation efficiency.

Generalizing the small-scale complexity of the hydrological system with these assumptions enable an application of the proposed framework for spatially distributed soil water balance simulations both to other farming systems and for the low-threshold implementation into PI strategies. Although the proposed framework allows for the ex-post identification of inappropriate values of I_{gross} (i.e., SWC deficits or water savings), its applicability is still limited to (i) large data and processing requirements compared to data-driven or empirical approaches, and (ii) a lacking straightforward solution to the key questions of irrigation scheduling, i.e., how much and when to irrigate (USDA, 1997).

In this study, the overall farm-scale computational time (on a personal computer with a CPU of 3.60 GHz and 64 GB RAM) amounted to approximately 2.5 days and by far exceeds the available time for irrigation scheduling in agricultural practice. However, irrigation is usually scheduled on specific (sub-) fields rather than on the entire farm simultaneously, depending on the available amount of irrigation systems. A computational time of approximately 2.25 min ha^{-1} and 1.09 min per 1D soil column indeed slightly exceeds the computational time presented in other studies (e.g., Mao et al., 2021; Rezaei et al., 2017) but is more suitable for practical application.

In addition, the proposed framework lacks a forward-running simulation of the soil water balance, mainly due to a limited accuracy of high-resolution weather forecasts. The simulation of different components of the soil water balance can nonetheless still constitute the basis for a spatially distributed irrigation scheduling. Particularly, the required location-specific values of I_{gross} to restore optimum crop water availability can be obtained by comparing the actual SWC with the crop-specific optimum PAW ranges. The irrigation timing can be enhanced by comparing simulated values of K(h) with the current SWC to estimate when the SWC drops below the lower threshold of optimum PAW.

Decreasing the spatial resolution could further enhance the applicability of spatially distributed soil water balance simulations but also further amplifies the above-mentioned generalization of the complexity of water flow dynamics within the root-zone of a crop. Alternatively, the

distribution of the proposed approach across a cluster or server infrastructure may considered a potential solution to reduce the runtime duration. Here, the development of our simulation framework with open-source technologies greatly simplifies an application to other farming systems and a further development of stand-alone applications, for instance.

4.4.2. Prospects for future research

Future research could therefore particularly focus on the use of spatially distributed HYDRUS-1D simulations to assess how much and when irrigation is needed. An integration of the proposed framework into existing irrigation decision support systems may aid in reducing the required efforts for data pre- and post-processing. An additional objective could be to investigate whether surface RS-SWC data or ET_C estimates derived from multispectral or thermal RS data can be used as input or calibration parameters in spatially distributed soil water balance simulations.

The fusion of HYDRUS-1D simulations with these RS information leverages the strengths of both data types: the field-based process modeling with HYDRUS-1D and the spatio-temporal capabilities from RS-data. Freely available datasets can mitigate both the challenge of generating high-resolution SWC observations at deeper soil layers using RS and the large data requirements of complex soil water balance simulations across spatio-temporal scales (Guo et al., 2023). In this context, Yu et al. (2022) and Zha et al. (2025) have already found that using RS data sets to optimize parameters when solving the Richards equation significantly improves the model accuracy for different soil textures and crops. The most frequently discussed approach to relate remotely-sensed surface SWC with the infiltration process of water in the soil profile is the exponential filter method (Wagner, 1998). Currently, the exponential filter method is particularly used to derive the "Soil Water Index", which may considered useful for PI due to the estimation of depth-specific SWC. However, the spatial resolution of 1 km limits its suitability for PI to capture small-scale heterogeneities in the soil water balance. Future research may hence investigate how novel procedures for spatial downscaling (Mahmood et al., 2024) may amplify the use of the "Soil Water Index" as an input or calibration parameter for the application of HYDRUS-1D in a spatially distributed manner.

4.4.3. Evaluation of research aims

Using combined a-priori information on depth-specific soil physical properties, meteorological conditions, location-specific values of I_{gross}, and phenological characteristics, this study applied the HYDRUS-1D software environment in a spatially distributed manner to derive accurate, high-resolution (70 m) and depth-specific simulations of different components of the soil water balance (SWC, PAW, ET_C, subsurface fluxes, root water uptake). In the context of PI, the proposed framework overcomes major limitations of previous approaches and may hence considered a feasible alternative approach. Among others, in-situ measurements are limited to inaccurately capturing the in-field specific variabilities of the soil water balance, RS-SWC data sets are limited to the sole representation of surface (~0 cm to 5 cm) SWC and a coarse spatial resolution, simple ET_C-based models solely focus on single components of the soil water balance instead of comprehensive simulations, and complex, more-dimensional soil water balance simulations are limited to large data and processing requirements.

In particular, although advantageous in the regular, contact-free and low-effort mapping of SWC on larger scales, the suitability of freely available remotely-sensed data sets of surface SWC for PI is limited by a coarse spatial resolution of > 1 km, which does not account for spatial heterogeneities in environmental conditions. Accordingly, two freely available data sets (SMAP-1km, Sentinel-1 soil water content) were less accurate than HYDRUS-1D simulations in this study, in comparison to in-situ measurements. Indeed, as RS-SWC wascapable of illustrating the mid-term temporal patterns of surface SWC, they may hence considered useful for the monitoring of agricultural droughts on larger scales. To increase the applicability of RS-SWC for the purpose of PI, novel algorithms are required to either downscale the raw satellite imagery to higher spatial resolution, or to fuse the surface observations with physically-based models to account for the requirement of depth-specific soil water balance estimates.

The suitability and contribution of complex soil water balance simulations for PI were explored by an estimation of spatially distributed values of the irrigation efficiency and potentials for farm-level water savings. Spatially distributed irrigation efficiencies provided valuable insights on the crop-specific ratio between I_{used} and I_{gross}. The estimation of potential farm-level water savings based on cumulative surpluses and deficits of SWC highlighted the appropriateness of an optimized I_{gross} of potatoes, wheat and sugar beet, which may increase the irrigability of other crops. Although the derived estimates are specific for the investigated fields of an existing farm, the availability of spatially distributed data sets on soil physical properties, meteorological conditions and phenological characteristics enable an application of the proposed framework also to other farming systems.

5. Conclusions

Understanding the spatio-temporal dynamics of the soil water balance provides essential insights for assessing the adequacy and sustainability of precision irrigation in heterogeneous landscapes. Complex physically-based models enable a precise simulation of different components of the soil water balance but require large efforts for data processing and parameterization. In this study, a novel framework was proposed for the application of one-dimensional numerical soil water balance simulations in a spatially distributed manner. This framework was evaluated against other approaches considered for precision irrigation (in-situ measurements and remotely-sensed observations) and provided accurate, high-resolution and depth-specific simulations of different components of the soil water balance (soil water content, plant available water content, crop evapotranspiration, subsurface fluxes, root water uptake) across an existing farm. Reliable contributions of the proposed framework for precision irrigation were furthermore derived from spatially distributed irrigation performance indicators. Beyond the farm-scale characteristics addressed in this study, the proposed framework supports broader water-policy objectives: the ability to quantify the irrigation efficiency and avoidable water losses based on numerical soil water balance simulations is directly relevant for sustainable quantitative water management under the EU Water Framework Directive and contributes to SDG 6.4. on improving the water-use efficiency in agriculture.

CRediT authorship contribution statement

Jan Lukas Wenzel: Writing – original draft, Visualization, Validation, Software, Methodology, Investigation, Formal analysis, Data curation, Conceptualization. **Christopher Conrad:** Writing – review & editing, Supervision, Project administration, Funding acquisition, Conceptualization. **Talha Mahmood:** Writing – review & editing, Data curation. **Matthias Kunz:** Project administration, Funding acquisition. **Martin Volk:** Writing – review & editing, Supervision. **Julia Pöhlitz:** Writing – review & editing, Supervision, Funding acquisition, Conceptualization.

Funding

This work is supported by funds of the Federal Ministry of Food and Agriculture (BMEL) based on a decision of the Parliament of the Federal Republic of Germany. The Federal Office for Agriculture and Food (BLE) supplies coordinating support for digitalization in agriculture as funding organization, grant number: FKZ 28DE114E18 & FKZ 28DE114A22.

Declaration of Competing Interest

The authors declare that they have no known competing financial interests or personal relationships that could have appeared to influence the work reported in this paper.

Acknowledgements

We highly appreciate the opportunity to conduct field experiments and field measurements on two fields of the farm in Mecklenburg-Western Pomerania, Germany, in accordance with standard cultivation practice. We express our thanks to the local farmer for providing us with all relevant information. We thank the "AgriSens-DEMMIN 4.0" project team for scientific and technical assistance within the DEMMIN (Durable Environmental Multidisciplinary Monitoring Information Network) study area. Mr. Michael von Hoff and Ms. Silke Kurze are appreciated for their assistance in laboratory work.

Appendix A. Supporting information

Supplementary data associated with this article can be found in the online version at doi:10.1016/j.agwat.2026.110157.

Data availability

Data will be made available on request.

References

Acharya, S., 2020. hydrusR: Utility package to run HYDRUS-1D and analyse results v.0.3.0 (Version 0.3.0) [software]. GitHub. ⟨https://github.com/shoebodh/hydrusR⟩.

Allen, R.G., Pereira, L.S., Raes, D., Smith, M., 1998. Crop evapotranspiration. Guidelines for computing crop water requirements. Food and Agriculture Organization of the United Nations, Rome. Italy.

Balenzano, A., Mattia, F., Satalino, G., Lovergine, F.P., Palmisano, D., Peng, J., Marzahn, P., Wegmüller, U., Cartus, O., Dąbrowska-Zielińska, K., Musial, J.P., Davidson, M.W.J., Pauwels, V.R.N., Cosh, M.H., McNairn, H., Johnson, J.T., Walker, J.P., Yueh, S.H., Entekhabi, D., Kerr, Y.H., Jackson, T.J., 2021. Sentinel-1 soil moisture at 1 km resolution: a validation study. Remote Sens. Environ. 263, 112554. https://doi.org/10.1016/j.rse.2021.112554.

Bauer-Marschallinger, B., Paulik, C., Hochstöger, S., Mistelbauer, T., Modanesi, S., Ciabatta, L., Massari, C., Brocca, L., Wagner, W., 2018. Soil moisture from fusion of scatterometer and SAR: closing the scale gap with temporal filtering. Remote Sens 10. https://doi.org/10.3390/rs10071030.

Beaudette, D., Skovlin, J., Andrew, B., 2024. soilDB: Soil Database Interface R package version v.2.8.13 (Version 2.8.13) [software]. ⟨https://CRAN.R-project.org/package=soilDB⟩.

Bos, M.G., Wolters, W., 1990. Water charges and irrigation efficiencies. Irrig. Drain. Syst. 4, 267–278. https://doi.org/10.1007/BF01117746.

Brocca, L., Tarpanelli, A., Filippucci, P., Dorigo, W., Zaussinger, F., Gruber, A., Fernandez-Prieto, D., 2018. How much water is used for irrigation? A new approach exploiting coarse resolution satellite soil moisture products. Int. J. Appl. Earth Obs. Geoinf. 73, 752–766. https://doi.org/10.1016/j.jag.2018.08.023.

Bublitz, T.A., Kemper, R., Müller, P., Kautz, T., Döring, T.F., Athmann, M., 2022. Relating Profile Wall Root-Length Density Estimates to Monolith Root-Length Density Measurements of Cover Crops. Agronomy 12. https://doi.org/10.3390/agronomy12010048.

Burt, C.M., Clemmens, A.J., Strelkoff, T.S., Solomon, K.H., Bliesner, R.D., Hardy, L.A., Howell, T.A., Eisenhauer, D.E., 1997. Irrigation Performance Measures: Efficiency and Uniformity. J. Irrig. Drain. Eng. 123, 423–442. https://doi.org/10.1061/(ASCE)0733-9437(1997)123:6(423).

Burth, U., Freier, B., 1999. Zur guten fachlichen Praxis im Pflanzenschutz. FAO AGRIS Int. Syst. Agric. Sci. Technol. 1, 5–8.

Chauhdary, J.N., Li, H., Jiang, Y., Pan, X., Hussain, Z., Javaid, M., Rizwan, M., 2024. Advances in Sprinkler Irrigation: A Review in the Context of Precision Irrigation for Crop Production. Agronomy 14. https://doi.org/10.3390/agronomy14010047.

Colliander, A., Jackson, T.J., Bindlish, R., Chan, S., Das, N., Kim, S.B., Cosh, M.H., Dunbar, R.S., Dang, L., Pashaian, L., Asanuma, J., Aida, K., Berg, A., Rowlandson, T., Bosch, D., Caldwell, T., Caylor, K., Goodrich, D., Jassar, H. al, Lopez-Baeza, E., Martínez-Fernández, J., González-Zamora, A., Livingston, S., McNairn, H., Pacheco, A., Moghaddam, M., Montzka, C., Notarnicola, C., Niedrist, G., Pellarin, T., Prueger, J., Pulliainen, J., Rautiainen, K., Ramos, J., Seyfried, M., Starks, P., Su, Z., Zeng, Y., Velde, R. van der, Thibeault, M., Dorigo, W., Vreugdenhil, M., Walker, J.P., Wu, X., Monerris, A., O'Neill, P.E., Entekhabi, D., Njoku, E.G., Yueh, S., 2017. Validation of SMAP surface soil moisture products with core validation sites. Remote Sens. Environ. 191, 215–231. https://doi.org/10.1016/j.rse.2017.01.021.

Conrad, C., Usman, M., Morper-Busch, L., Schönbrodt-Stitt, S., 2020. Remote sensing-based assessments of land use, soil and vegetation status, crop production and water use in irrigation systems of the Aral Sea Basin. A review. Water Secur 11, 100078. https://doi.org/10.1016/j.wasec.2020.100078.

Cordel, J., Anlauf, R., Prämaßing, W., Broll, G., 2025. Predicting water distribution and optimizing irrigation management in Turfgrass rootzones using HYDRUS-2D. Hydrology 12. https://doi.org/10.3390/hydrology12030053.

Costanzo, C., Costabile, P., Gangi, F., Argirò, G., Bautista, E., Gandolfi, C., Masseroni, D., 2024. Promoting precision surface irrigation through hydrodynamic modelling and microtopographic survey. Agric. Water Manag 301, 108950. https://doi.org/10.1016/j.agwat.2024.108950.

Ehrhardt, A., Groh, J., Gerke, H.H., 2025. Effects of different climatic conditions on soil water storage patterns. Hydrol. Earth Syst. Sci. 29, 313–334. https://doi.org/10.5194/hess-29-313-2025.

El Hajj, M., Baghdadi, N., Zribi, M., Bazzi, H., 2017. Synergetic use of Sentinel-1 and Sentinel-2 images for operational soil moisture mapping at high spatial resolution over agricultural areas. Remote Sens. 9, 1292. https://doi.org/10.3390/rs9121292.

Er-Raki, S., Ezzahar, J., Merlin, O., Amazirh, A., Hssaine, B.A., Kharrou, M.H., Khabba, S., Chehbouni, A., 2021. Performance of the HYDRUS-1D model for water balance components assessment of irrigated winter wheat under different water managements in semi-arid region of Morocco. Agric. Water Manag. https://doi.org/10.1016/j.agwat.2020.106546.

European Space Agency, 2022. SENTINEL-1B In-Flight Anomaly Summary Report. European Space Agency, Paris, France.

Fan, D., Zhao, T., Jiang, X., García-García, A., Schmidt, T., Samaniego, L., Attinger, S., Wu, H., Jiang, Y., Shi, J., Fan, L., Tang, B.-H., Wagner, W., Dorigo, W., Gruber, A., Mattia, F., Balenzano, A., Brocca, L., Jagdhuber, T., Wigneron, J.-P., Montzka, C., Peng, J., 2025a. A Sentinel-1 SAR-based global 1-km resolution soil moisture data product: Algorithm and preliminary assessment. Remote Sens. Environ. 318, 114579. https://doi.org/10.1016/j.rse.2024.114579.

Fan, D., Zhao, T., Jiang, X., García-García, A., Schmidt, T., Samaniego, L., Attinger, S., Wu, H., Jiang, Y., Shi, J., Fan, L., Tang, B., Wagner, W., Dorigo, W., Gruber, A., Mattia, F., Balenzano, A., Brocca, L., Jagdhuber, T., Wigneron, J.-P., Montzka, C., Peng, J., 2025b. A global soil moisture product at 1 km resolution based on Sentinel-1 (2016-2022) [dataset]. PANGAEA. https://doi.org/10.1594/PANGAEA.968754.

Fang, B., Lakshmi, V., Cosh, M., Liu, P.-W., Bindlish, R., Jackson, T.J., 2022. A global 1-km downscaled SMAP soil moisture product based on thermal inertia theory. Vadose Zone J. 21, e20182. https://doi.org/10.1002/vzj2.20182.

Feddes, R.A., Kowalik, P.J., Zaradny, H., 1978. Simulation of Field Water Use and Crop Yield. John Wiley & Sons, INC, New York, NY, USA, NY.

Fritsch, S., Machwitz, M., Ehammer, A., Conrad, C., Dech, S., 2012. Validation of the collection 5 MODIS FPAR product in a heterogeneous agricultural landscape in arid Uzbekistan using multitemporal RapidEye imagery. Int. J. Remote Sens 33, 6818–6837. https://doi.org/10.1080/01431161.2012.692834.

van Genuchten, M.T., 1980. A closed-form Equation for Predicting the Hydraulic-Conductivity of Unsatured Soils. Soil Sci. Soc. Am. J. 44, 892–898.

German Meteorological Service, 2017. DWD Wettershop—agrowetter beregnung.

German Meteorological Service, 2024. Open Climate Data Portal. ⟨https://opendata.dwd.de/⟩ (accessed 17 December 2024).

Ghazouani, H., Rallo, G., Mguidiche, A., Latrech, B., Douh, B., Boujelben, A., Provenzano, G., 2019. Assessing Hydrus-2D Model to Investigate the Effects of Different On-Farm Irrigation Strategies on Potato Crop under Subsurface Drip Irrigation. Water 11. https://doi.org/10.3390/w11030540.

Gibon, F., Mialon, A., Richaume, P., Rodríguez-Fernández, N., Aberer, D., Boresch, A., Crapolicchio, R., Dorigo, W., Gruber, A., Himmelbauer, I., Preimesberger, W., Sabia, R., Stradiotti, P., Tercjak, M., Kerr, Y.H., 2024. Estimating the uncertainties of satellite derived soil moisture at global scale. Sci. Remote Sens 10, 100147. https://doi.org/10.1016/j.srs.2024.100147.

Görz, G., Hock, A., 1939. Reichsbodenschätzung und Bodenkunde. Z. Dtsch. Geol. Ges. 91, 612–616.

Gu, Z., Qi, Z.M., Burghate, R., Yuan, S.Q., Jiao, X.Y., Xu, J.Z., 2020. Irrigation Scheduling Approaches and Applications: A Review. J. Irrig. Drain. Eng. 146, 04020007. https://doi.org/10.1061/(ASCE)IR.1943-4774.0001464.

Guo, X., Fang, X., Zhu, Q., Jiang, S., Tian, J., Tian, Q., Jin, J., 2023. Estimation of Root-Zone Soil Moisture in Semi-Arid Areas Based on Remotely Sensed Data. Remote Sens 15. https://doi.org/10.3390/rs15082003.

Haghverdi, A., Leib, B.G., Washington-Allen, R.A., Buschermohle, M.J., Ayers, P.D., 2016. Studying uniform and variable rate center pivot irrigation strategies with the aid of site-specific water production functions. Comput. Electron. Agric. 123, 327–340. https://doi.org/10.1016/j.compag.2016.03.010.

Hartmann, K.J., Bauriegel, A., Dehner, U., Eberhardt, E., Hesse, S., Kühn, D., Martin, W., Waldmann, F., 2024. In: Boden, A.G., Hannover, B.G.R. (Eds.), Bodenkundliche Kartieranleitung KA6 in 2 Bänden, Sixth ed. Schweizerbart Science Publishers, Stuttgart, Germany.

Howell, T.A., 2003. Irrigation Efficiency. In: Encyclopedia of Water Science. Marcel Dekker, Inc, New York, NY, USA.

Huang, J., Sehgal, V., Alvarez, L.V., Brocca, L., Cai, S., Cheng, R., Cheng, X., Du, J., El Masri, B., Endsley, K.A., Fang, Y., Hu, J., Jampani, M., Kibria, M.G., Koren, G., Li, L., Liu, L., Mao, J., Moreno, H.A., Rigden, A., Shi, M., Shi, X., Wang, Y., Zhang, X., Fisher, J.B., 2025. Remotely Sensed High-Resolution Soil Moisture and Evapotranspiration: Bridging the Gap Between Science and Society. Water Resour. Res. 61, e2024WR037929. https://doi.org/10.1029/2024WR037929.

Ionita, M., Nagavciuc, V., 2021. Changes in drought features at the European level over the last 120 years. Nat. Hazards Earth Syst. Sci. 21, 1685–1701. https://doi.org/10.5194/nhess-21-1685-2021.

IUSS Working Group WRB, 2015. World Reference Base for Soil Resources 2014, Update 2015. World Soil Resources Report No. 106. FAO, Rome.
Jensen, M.E., Swarner, L.R., Phelan, J.T., 1967. Improving Irrigation Efficiencies. In: Hagan, R.M., Haise, H.R., Phelan, J.T. (Eds.), Irrigation of Agricultural Lands. John Wiley & Sons, Ltd, pp. 1120–1142. https://doi.org/10.2134/agronmonogr11.c66.
Jones, J.W., Hoogenboom, G., Porter, C.H., Boote, K.J., Batchelor, W.D., Hunt, L.A., Wilkens, P.W., Singh, U., Gijsman, A.J., Ritchie, J.T., 2003. The DSSAT cropping system model. In: Eur. J. Agron, 18, pp. 235–265. https://doi.org/10.1016/S1161-0301(02)00107-7.
Kandelous, M.M., Šimůnek, J., 2010. Numerical simulations of water movement in a subsurface drip irrigation system under field and laboratory conditions using HYDRUS-2D. Agric. Water Manag. 97, 1070–1076. https://doi.org/10.1016/j.agwat.2010.02.012.
Kemper, R., Döring, T.F., Legner, N., Meinen, C., Athmann, M., 2022. Root traits in cover crop mixtures of blue lupin and winter rye. Plant Soil 475, 309–328. https://doi.org/10.1007/s11104-022-05366-9.
Kharrou, M.H., Simonneaux, V., Er-Raki, S., Le Page, M., Khabba, S., Chehbouni, A., 2021. Assessing Irrigation Water Use with Remote Sensing-Based Soil Water Balance at an Irrigation Scheme Level in a Semi-Arid Region of Morocco. Remote Sens 13. https://doi.org/10.3390/rs13061133.
Kisekka, I., Peddinti, S.R., Kustas, W.P., McElrone, A.J., Bambach-Ortiz, N., McKee, L., Bastiaanssen, W., 2022. Spatial–temporal modeling of root zone soil moisture dynamics in a vineyard using machine learning and remote sensing. Irrig. Sci. 40, 761–777. https://doi.org/10.1007/s00271-022-00775-1.
Kool, J.B., Parker, J.C., Genuchten, M.T. van, 1987. Parameter estimation for unsaturated flow and transport models — A review. J. Hydrol. 91, 255–293. https://doi.org/10.1016/0022-1694(87)90207-1.
Kragh, S.J., Dari, J., Modanesi, S., Massari, C., Brocca, L., Fensholt, R., Stisen, S., Koch, J., 2024. An inter-comparison of approaches and frameworks to quantify irrigation from satellite data. Hydrol. Earth Syst. Sci. 28, 441–457. https://doi.org/10.5194/hess-28-441-2024.
Kumar, H., Srivastava, P., Lamba, J., Diamantopoulos, E., Ortiz, B., Morata, G., Takhellambam, B., Bondesan, L., 2022. Site-specific irrigation scheduling using one-layer soil hydraulic properties and inverse modeling. Agric. Water Manag 273, 107877. https://doi.org/10.1016/j.agwat.2022.107877.
Kuznetsov, M., Yakirevich, A., Pachepsky, Y.A., Sorek, S., Weisbrod, N., 2012. Quasi 3D modeling of water flow in vadose zone and groundwater. J. Hydrol. 450–451, 140–149. https://doi.org/10.1016/j.jhydrol.2012.05.025.
Lakshmi, V., Fang, B., 2023. SMAP-Derived 1-km Downscaled Surface Soil Moisture Product, Version 1 [dataset]. https://doi.org/10.5067/U8QZ2AXE5V7B. (accessed 12 August 2025.
Lazarovitch, N., Kisekka, I., Oker, T.E., Brunetti, G., Wöhling, T., Xianyue, L., Yong, L., Skaggs, T.H., Furman, A., Sasidharan, S., Raij-Hoffman, I., Šimůnek, J., 2023. Chapter Two - Modeling of irrigation and related processes with HYDRUS. In: Sparks, D.L. (Ed.), Advances in Agronomy, 181. Academic Press, p. 79. https://doi.org/10.1016/bs.agron.2023.05.002.
Li, M., Sun, H., Zhao, R., 2023. A Review of Root Zone Soil Moisture Estimation Methods Based on Remote Sensing. Remote Sens 15. https://doi.org/10.3390/rs15225361.
Liebhard, G.C., Klik, A., Stumpp, C., Morales Santos, A.G., Eitzinger, J., Nolz, R., 2022. Estimation of evaporation and transpiration rates under varying water availability for improving crop management of soybeans using oxygen isotope ratios of pore water. Int Agrophys 36, 181–195. https://doi.org/10.31545/intagr/150811.
Mahmood, T., Löw, J., Pöhlitz, J., Wenzel, J.L., Conrad, C., 2024. Estimation of 100 m root zone soil moisture by downscaling 1 km soil water index with machine learning and multiple geodata. Environ. Monit. Assess. 196, 823. https://doi.org/10.1007/s10661-024-12969-5.
Mao, W., Zhu, Y., Ye, M., Zhang, X., Wu, J., Yang, J., 2021. A new quasi-3-D model with a dual iterative coupling scheme for simulating unsaturated-saturated water flow and solute transport at a regional scale. J. Hydrol. 602, 126780. https://doi.org/10.1016/j.jhydrol.2021.126780.
Marquardt, D.W., 1963. An Algorithm for Least-Squares Estimation of Nonlinear Parameters. J. Soc. Ind. Appl. Math. 11, 431–441. https://doi.org/10.1137/0111030.
Massart, S., Vreugdenhil, M., Bauer-Marschallinger, B., Navacchi, C., Raml, B., Wagner, W., 2024. Mitigating the impact of dense vegetation on the Sentinel-1 surface soil moisture retrievals over Europe. Eur. J. Remote Sens 57, 2300985. https://doi.org/10.1080/22797254.2023.2300985.
de Mendiburu, F., 2023. agricolae: Statistical procedures for Agricultural Research.
Michel, R., Dannowski, R., 2013. Using Soil–Water–Plant Models to Improve the Efficiency of Irrigation. In: Müller, L., Saparov, A., Lischeid, G. (Eds.), Novel Measurement and Assessment Tools for Monitoring and Management of Land and Water Resources in Agricultural Landscapes of Central Asia. Springer, Heidelberg, New York, Dordrecht, London, pp. 379–388. https://doi.org/10.1007/978-3-319-01017-5_22.
Mualem, Y., 1976. A new model for precidicting the hydraulic conductivity of unsatured porous media. Water Resour. Res. 12, 513–522.
Myneni, R.B., Hoffman, S., Knyazikhin, Y., Privette, J.L., Glassy, J., Tian, Y., Wang, Y., Song, X., Zhang, Y., Smith, G.R., Lotsch, A., Friedl, M., Morisette, J.T., Votava, P., Nemani, R.R., Running, S.W., 2002. Global products of vegetation leaf area and fraction absorbed PAR from year one of MODIS data. Remote Sens. Environ. 83, 214–231. https://doi.org/10.1016/S0034-4257(02)00074-3.
Peng, J., Albergel, C., Balenzano, A., Brocca, L., Cartus, O., Cosh, M.H., Crow, W.T., Dabrowska-Zielinska, K., Dadson, S., Davidson, M.W.J., Rosnay, P. de, Dorigo, W., Gruber, A., Hagemann, S., Hirschi, M., Kerr, Y.H., Lovergine, F., Mahecha, M.D., Marzahn, P., Mattia, F., Musial, J.P., Preuschmann, S., Reichle, R.H., Satalino, G., Silgram, M., Bodegom, P.M. van, Verhoest, N.E.C., Wagner, W., Walker, J.P., Wegmüller, U., Loew, A., 2021. A roadmap for high-resolution satellite soil moisture applications – confronting product characteristics with user requirements. Remote Sens. Environ. 252, 112162. https://doi.org/10.1016/j.rse.2020.112162.
Pereira, H., Marques, R.C., 2017. An analytical review of irrigation efficiency measured using deterministic and stochastic models. Agric. Water Manag 184, 28–35. https://doi.org/10.1016/j.agwat.2016.12.019.
Pereira, L.S., Paredes, P., Jovanovic, N., 2020. Soil water balance models for determining crop water and irrigation requirements and irrigation scheduling focusing on the FAO56 method and the dual K-c approach. Agric. Water Manag 241, 106357. https://doi.org/10.1016/j.agwat.2020.106357.
Petrović, B., Bumbálek, R., Zoubek, T., Kuneš, R., Smutný, L., Bartoš, P., 2024. Application of precision agriculture technologies in Central Europe-review. J. Agric. Food Res. 15, 101048. https://doi.org/10.1016/j.jafr.2024.101048.
Phillips, A.J., Newlands, N.K., Liang, S.H.L., Ellert, B.H., 2014. Integrated sensing of soil moisture at the field-scale: Measuring, modeling and sharing for improved agricultural decision support. Comput. Electron. Agric. 107, 73–88. https://doi.org/10.1016/j.compag.2014.02.011.
Pierce, F.J., 2010. Precision Irrigation. Landbauforsch Völkenrode 45–56.
Piernicke, T., Kunz, M., Itzerott, S., Wenzel, J.L., Pöhlitz, J., Conrad, C., 2025. A Spatially Comprehensive Water Balance Model for Starch Potato from Combining Multispectral Ground Station and Remote Sensing Data in Precision Agriculture. Remote Sens 17. https://doi.org/10.3390/rs17183227.
Poggio, L., de Sousa, L.M., Batjes, N.H., Heuvelink, G.B.M., Kempen, B., Ribeiro, E., Rossiter, D., 2021. SoilGrids 2.0: producing soil information for the globe with quantified spatial uncertainty. SOIL 7, 217–240. https://doi.org/10.5194/soil-7-217-2021.
Raes, D., Steduto, P., Hsiao, T.C., Fereres, E., 2023. AquaCrop Version 7.1 - Reference manual - Chapter 1 - FAO crop-water productivity model to simulate yield response to water. FAO - Food and Agriculture Organization of the United Nations, Rome.
Ray, R.L., Fares, A., He, Y., Temimi, M., 2017. Evaluation and Inter-Comparison of Satellite Soil Moisture Products Using In Situ Observations over Texas, U.S. Water 9. https://doi.org/10.3390/w9060372.
Reichle, R.H., Liu, Q., Koster, R.D., Crow, W.T., De Lannoy, G.J.M., Kimball, J.S., Ardizzone, J.V., Bosch, D., Colliander, A., Cosh, M., Kolassa, J., Mahanama, S.P., Prueger, J., Starks, P., Walker, J.P., 2019. Version 4 of the SMAP Level-4 Soil Moisture Algorithm and Data Product. J. Adv. Model. Earth Syst. 11, 3106–3130. https://doi.org/10.1029/2019MS001729.
Rey, D., Holman, I.P., Daccache, A., Morris, J., Weatherhead, E.K., 2016. Modelling and mapping the economic value of supplemental irrigation in a humid climate. Agric. Water Manag 173, 13–22.
Rezaei, M., Pue, J.D., Seuntjens, P., Joris, I., Cornelis, W., 2017. Quasi 3D modelling of vadose zone soil-water flow for optimizing irrigation strategies: Challenges, uncertainties and efficiencies. Environ. Model. Softw. 93, 59–77. https://doi.org/10.1016/j.envsoft.2017.03.008.
Richards, L.A., 1931. Capillary conduction of liquids through porous mediums. Physics 1, 318–333.
Riediger, J., Breckling, B., Nuske, R.S., Schröder, W., 2014. Will climate change increase irrigation requirements in agriculture of Central Europe? A simulation study for Northern Germany. Environ. Sci. Eur. 26, 18. https://doi.org/10.1186/s12302-014-0018-1.
Rochester, E.W., 2017. Glossary of Irrigation Terms. Irrigation Association.
Rogers, D.H., 1997. Efficiencies and water losses of irrigation systems. Coop. Ext. Serv. Kans. State Univ.
Sadler, E.J., Evans, R.G., Stone, K.C., Camp, C.R., 2005. Opportunities for conservation with precision irrigation. J. Soil Water Conserv 60, 371–378. https://doi.org/10.1080/00224561.2005.12435829.
Schaap, M.G., Leij, F.J., van Genuchten, M.Th, 2001. ROSETTA: a computer program for estimating soil hydraulic parameters with hierarchical pedotransfer functions. J. Hydrol. 251, 163–176.
Senanayake, I.P., Pathira Arachchilage, K.R.L., Yeo, I.-Y., Khaki, M., Han, S.-C., Dahlhaus, P.G., 2024. Spatial Downscaling of Satellite-Based Soil Moisture Products Using Machine Learning Techniques: A Review. Remote Sens 16. https://doi.org/10.3390/rs16122067.
Šimunek, J., Hopmans, J.W., Nielsen, D.R., Th, van Genuchten, M., 2000. Horizontal Infiltration revisited using Parameter Estimation. Soil Sci. 165.
Šimůnek, J., van Genuchten, M.T., Sejna, M., 2005. The HYDRUS-1D Software package for simulating the one-dimensional movement of water, heat, and multiple solutes in variably-saturated media, University of California-Riverside Research Reports. University of California, Riverside, CA, USA.
Šimůnek, J., van Genuchten, M.T., Šejna, M., 2012a. HYDRUS: Model Use, Calibration, and Validation. Trans. ASABE 55, 1263. https://doi.org/10.13031/2013.42239.
Šimůnek, J., van Genuchten, M.T., Šejna, M., 2012b. The HYDRUS Software Package for Simulating the Two- and Three-Dimensional Movement of Water, Heat, and Multiple Solutes in Variably-Saturated Porous Media, University of California-Riverside Research Reports. University of California, Riverside, CA, USA.
Smith, M., 1992. CROPWAT. A computer programme for irrigation planning and management. Food and Agriculture Organization of the United Nations, Rome. Italy.
Song, C., Zhang, D., Jing, Z., Nie, X., Di, B., Qian, J., Cheng, W., Zhang, G., Shan, G., 2025. Field Experimental Assessment of HYDRUS-3D Soil Moisture Simulations Under Drip Irrigation Using Horizontal Mobile Dielectric Sensor. Agronomy 15. https://doi.org/10.3390/agronomy15040776.
Spengler, D., Asam, S., Böttcher, F., Borg, E., Dobers, E.S., Geßner, U., Harfenmeister, K., Hüttich, C., Klan, F., Teucher, M., Truckenbrodt, S., Conrad, C., 2021. Einsatz von Fernerkundungstechnologien für die Digitalisierung im Pflanzenbau. In: Meyer-Aurich, A., Gandorfer, M., Hoffmann, C., Weltzien, C., Bellingrath-Kimura, S., Floto, H. (Eds.), 41. GIL-Jahrestagung, Informations- Und

Kommunikationstechnologie in Kritischen Zeiten. Presented at the Gesellschaft für Informatik e.V., Bonn, pp. 415–420.
Suman, S., Srivastava, P.K., Petropoulos, G.P., Pandey, D.K., O'Neill, P.E., 2020. Appraisal of SMAP Operational Soil Moisture Product from a Global Perspective. Remote Sens 12. https://doi.org/10.3390/rs12121977.
Sutanto, S.J., Wenninger, J., Coenders-Gerrits, A.M.J., Uhlenbrook, S., 2012. Partitioning of evaporation into transpiration, soil evaporation and interception: a comparison between isotope measurements and a HYDRUS-1D model. Hydrol. Earth Syst. Sci. 16, 2605–2616. https://doi.org/10.5194/hess-16-2605-2012.
Tenreiro, T.R., García-Vila, M., Gómez, J.A., Jimenez-Berni, J.A., Fereres, E., 2020. Water modelling approaches and opportunities to simulate spatial water variations at crop field level. Agric. Water Manag 240, 106254. https://doi.org/10.1016/j.agwat.2020.106254.
Tola, D., Bustillos, L., Arragan, F., Chipana, R., Hostache, R., Resongles, E., Espinoza-Villar, R., Zolá, R.P., Uscamayta, E., Perez-Flores, M., Satgé, F., 2025. High Spatial Resolution Soil Moisture Mapping over Agricultural Field Integrating SMAP, IMERG, and Sentinel-1 Data in Machine Learning Models. Remote Sens 17. https://doi.org/10.3390/rs17132129.
Tolk, J.A., Howell, T.A., Steiner, J.L., Krieg, D.R., Schneider, A.D., 1995. Role of transpiration suppression by evaporation of intercepted water in improving irrigation efficiency. Irrig. Sci. 16, 89–95. https://doi.org/10.1007/BF00189165.
USDA, 1997. Irrigation Guide (No. Part 652), National Engineering Handbook. United States Department of Agriculture (USDA), Washington, D.C.
Usman, M., Chua, L.H.C., Irvine, K.N., Teang, L., 2025. Numerical modelling of vadose zone flow for a shallow groundwater wetland using HYDRUS-1D. Model. Earth Syst. Environ. 11, 296. https://doi.org/10.1007/s40808-025-02472-2.
Ventrella, D., Castellini, M., Di Prima, S., Garofalo, P., Lassabatère, L., 2019. Assessment of the Physically-Based Hydrus-1D Model for Simulating the Water Fluxes of a Mediterranean Cropping System. Water 11. https://doi.org/10.3390/w11081657.
Vereecken, H., Weynants, M., Javaux, M., Pachepsky, Y., Schaap, M.G., Genuchten, M. Th. van, 2010. Using Pedotransfer Functions to Estimate the van Genuchten–Mualem Soil Hydraulic Properties: A Review. Vadose Zone J. 9, 795–820. https://doi.org/10.2136/vzj2010.0045.
Vereecken, H., Schnepf, A., Hopmans, J.W., Javaux, M., Or, D., Roose, T., Vanderborght, J., Young, M.H., Amelung, W., Aitkenhead, M., Allison, S.D., Assouline, S., Baveye, P., Berli, M., Brüggemann, N., Finke, P., Flury, M., Gaiser, T., Govers, G., Ghezzehei, T., Hallett, P., Hendricks Franssen, H.J., Heppell, J., Horn, R., Huisman, J.A., Jacques, D., Jonard, F., Kollet, S., Lafolie, F., Lamorski, K., Leitner, D., McBratney, A., Minasny, B., Montzka, C., Nowak, W., Pachepsky, Y., Padarian, J., Romano, N., Roth, K., Rothfuss, Y., Rowe, E.C., Schwen, A., Šimůnek, J., Tiktak, A., Van Dam, J., van der Zee, S.E.A.T.M., Vogel, H.J., Vrugt, J.A., Wöhling, T., Young, I.M., 2016. Modeling Soil Processes: Review, Key Challenges, and New Perspectives. Vadose Zone J. 15, vzj2015.09.0131. https://doi.org/10.2136/vzj2015.09.0131.
Vrugt, J.A., Stauffer, P.H., Woehling, Th, Robinson, B.A., Vesselinov, V.V., 2008. Inverse modeling of subsurface flow and transport properties: A review with new developments. Vadose Zone J. https://doi.org/10.2136/vzj2007.0078.
Wagner, W., 1998. Soil moisture retrieval from ERS scatterometer data, 49. Inst. für Photogrammetrie u. Fernerkundung d. Techn. Univ., Wien, Wien.
Wang, L., Qu, J.J., 2009. Satellite remote sensing applications for surface soil moisture monitoring: a review. Front. Earth Sci. China 3, 237–247. https://doi.org/10.1007/s11707-009-0023-7.
Wenzel, J.L., Conrad, C., Piernicke, T., Spengler, D., Pöhlitz, J., 2022. Assessing the Impact of Different Irrigation Levels on Starch Potato Production. Agronomy 12. https://doi.org/10.3390/agronomy12112685.
Wenzel, J.L., Pöhlitz, J., Usman, M., Piernicke, T., Conrad, C., 2025. Enhancing irrigation scheduling by application efficiency estimations and soil moisture simulations. Eur. J. Agron. 164, 127487. https://doi.org/10.1016/j.eja.2024.127487.
Wesseling, J.G., Elbers, J.A., Kabat, P., van den Broek, B.J., 1991. SWATRE: Instructions for Input, Report. Winand Staring Center, Wageningen, The Netherlands.
Westenbroek, S.M., Engott, J.A., Kelson, V.A., Hunt, R.J., 2018. SWB Version 2.0—A soil-water-balance code for estimating net infiltration and other water-budget components (Report No. 6-A59), Techniques and Methods. Reston, VA. https://doi.org/10.3133/tm6A59.
Yu, J., Wu, Y., Xu, L., Peng, J., Chen, G., Shen, X., Lan, R., Zhao, C., Zhangzhong, L., 2022. Evaluating the Hydrus-1D Model Optimized by Remote Sensing Data for Soil Moisture Simulations in the Maize Root Zone. Remote Sens 14. https://doi.org/10.3390/rs14236079.
Zaussinger, F., Dorigo, W., Gruber, A., Tarpanelli, A., Filippucci, P., Brocca, L., 2019. Estimating irrigation water use over the contiguous United States by combining satellite and reanalysis soil moisture data. Hydrol. Earth Syst. Sci. 23, 897–923. https://doi.org/10.5194/hess-23-897-2019.
Zha, X., Zhu, W., Han, Y., Lv, A., 2025. Enhancing root-zone soil moisture estimation using Richards' equation and dynamic surface soil moisture data. Agric. Water Manag 312, 109460. https://doi.org/10.1016/j.agwat.2025.109460.
Zhang, C., Long, D., 2021. Estimating Spatially Explicit Irrigation Water Use Based on Remotely Sensed Evapotranspiration and Modeled Root Zone Soil Moisture. Water Resour. Res. 57, e2021WR031382. https://doi.org/10.1029/2021WR031382.
Zhao, Y., Yi, J., Yao, R., Li, F., Hill, R.L., Gerke, H.H., 2024. Dimensionality and scales of preferential flow in soils of Shale Hills hillslope simulated using HYDRUS. Vadose Zone J. 23, e20367. https://doi.org/10.1002/vzj2.20367.
Zheng, C., Jia, L., Zhao, T., 2023. A 21-year dataset (2000–2020) of gap-free global daily surface soil moisture at 1-km grid resolution. Sci. Data 10, 139. https://doi.org/10.1038/s41597-023-01991-w.